THE JOURNAL OF PHYSICAL CHEMISTRY A

 VOLUME 110, NUMBER 12, MARCH 30, 2006

FEATURE ARTICLE

Laser Probes of Conformational Isomerization in Flexible Molecules and Complexes

Timothy S. Zwier†

Department of Chemistry, Purdue University, 560 Oval Drive, West Lafayette, Indiana 47907-2084

Received: November 4, 2005; In Final Form: December 23, 2005

Molecules with several flexible coordinates have potential energy surfaces with a large number of minima and many transition states separating them. A general experimental protocol is described that is capable of studying conformational isomerization in such circumstances, measuring the product quantum yields following conformation-specific infrared excitation, and measuring energy thresholds for isomerization of specific X → Y reactant-product isomer pairs following excitation via stimulated emission pumping (SEP). These methods have been applied to a series of molecules of varying size and conformational complexity, including 3-indolepropionic acid (IPA), *meta*-ethynylstyrene, *N*-acetyltryptophan methyl amide (NATMA), *N*-acetyltryptophan amide (NATA), and melatonin. Studies of isomerization in solute−solvent complexes are also described, including a measurement of the barrier to isomerization in the IPA−H_2O complex, and a unique isomerization reaction in which a single water molecule is shuttled between H-bonding sites on the *trans*-formanilide (TFA) molecule.

Introduction

The field of chemical dynamics, which seeks to understand how elementary unimolecular and bimolecular reactions occur, is founded on a rich tradition of accomplishment in studies of small molecules with a few internal degrees of freedom.[1−4] Among the powerful tools used to probe dynamics are state-specific measurements, which proceed by defining or restricting the reactant states and determining, to the extent possible, the product state distributions (electronic, vibration, rotation) that are thereby formed.[5−15] Out of such studies, rules have been formulated that relate the observed state-to-state propensities to features of the underlying potential energy surface on which the reaction takes place.[5]

Conformational isomerization is a special class of unimolecular reaction that involves hindered rotation about one or more flexible bonds. In cases where isomerization involves two conformational minima separated by a single barrier, state-specific studies of the process continue to be possible and are adding much to our understanding of the time scales and energy flow that accompanies isomerization.[16−20]

Conformational Isomerization and the Complexity Gap. As the size and chemical complexity of the molecule grows, conformational isomerization quickly evolves from motion along a single well-defined internal coordinate into a complicated motion on a multidimensional potential energy surface of substantial complexity. One measure of this complexity is

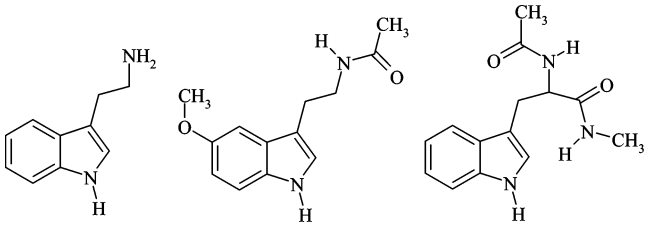

Tryptamine Melatonin N-acetyl tryptophan methyl amide (NATMA)

† E-mail: zwier@purdue.edu.

10.1021/jp056390z CCC: $33.50
Published on Web 02/28/2006

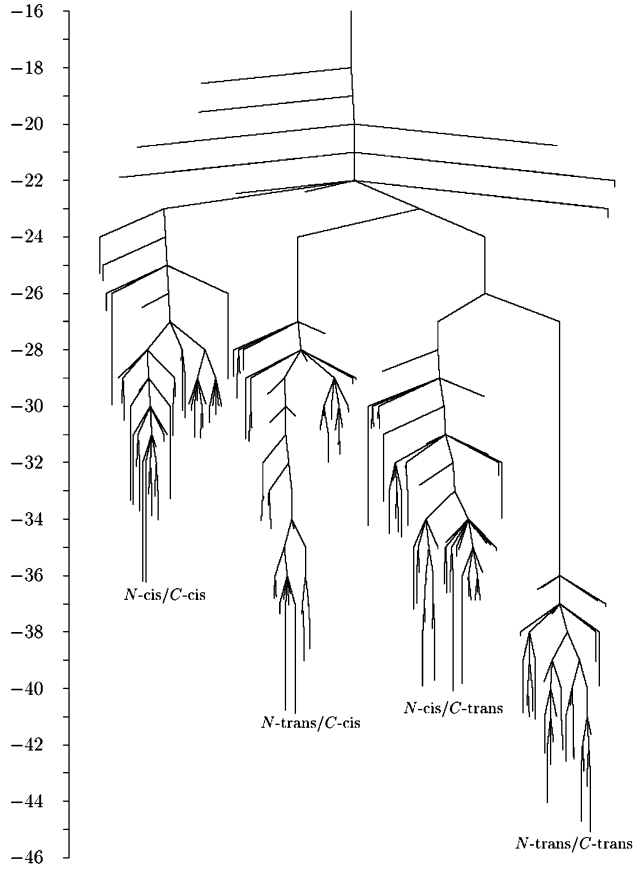

Figure 1. Disconnectivity diagram for NATMA using the AMBER force field and parm96.dat parameters.[23−25]

simply to count the number of conformational minima on the potential energy surface. The three molecules tryptamine, melatonin, and *N*-acetyl tryptophan methyl amide (NATMA), which are subjects of the present article, serve to illustrate the point. In tryptamine, the ethylamine side chain is sufficiently small that ab initio searches can be used to locate all 11 spectroscopically distinguishable minima and the transition states connecting them.[21]

The potential energy surface for melatonin, with its larger 3-ethylacetamido and small 5-methoxy side chains, is predicted by Csontos et al.[22] to have 128 conformational minima at the HF/6-31G* level of theory. Similarly, a search of the conformational space of NATMA using the AMBER force field (with parm96.dat parameters),[23,24] yields 164 minima.[25] Of course, many of these minima are quite high in energy, so that under typical thermal conditions they play no part in the molecule's conformational dynamics. Nevertheless, the tryptamine → melatonin → NATMA series illustrates clearly that even modest increases in the molecular size and number of flexible coordinates quickly leads to potential energy surfaces complex enough to intimidate even the bravest of experimentalists. Furthermore, the kinetics and dynamics of isomerization (e.g., the isomerization rates and key isomerization pathways) also depend critically on the energy barriers that separate these minima.

Disconnectivity diagrams provide useful visual summaries of all the conformational minima and transition states of flexible molecules.[26,27] Figure 1 presents the disconnectivity diagram for NATMA,[25] generated with the AMBER force field. In the diagram, the end of each branch identifies a particular conformational minimum, and the nodal points representing collections of transition states in the prescribed energy window that connect the minima below them.[26,27] Although such a diagram is of limited quantitative accuracy, it nicely illustrates the complexity of the potential energy surface for NATMA, with its 164 minima connected by 714 transition states.

Timothy Zwier is a professor of chemistry and department head at Purdue University in West Lafayette, IN. He received his B.S. from Calvin College in 1977 and his Ph.D. from the University of Colorado—Boulder in 1981. He subsequently spent two years as a postdoctoral research associate at the James Franck Institute of the University of Chicago before returning to Calvin College as an assistant professor in 1983. In 1988 he moved to Purdue University, where he and his research group have engaged in studies of the spectroscopy, dynamics, and photochemistry of isolated molecules and molecular clusters, including applications to combustion processes and planetary atmospheres.

By many standards, the molecular series just introduced is composed of molecules that are entirely too small to be of direct relevance to the analogous conformational isomerization process in large macromolecules such as proteins. However, for typical proteins with 100 or more residues, generating disconnectivity diagrams of all the stationary points on the potential energy landscape is extraordinarily challenging.[28,29] Furthermore, state-specific descriptions of the dynamics of folding in this macromolecule limit are clearly beyond our present grasp, whether experimentally or by calculation. The wide gulf in terminology, methodology, and goals for studies of conformational isomerization conducted in the two extremes of small and large constitutes a "complexity gap", which is currently of significant proportions.

It is in this context that molecules such as those shown above can play a role in forging a path into the complexity gap. Molecules in this complexity range are large enough to possess several flexible degrees of freedom, but small enough to still benefit from conformation-selective and state-selective studies of the conformational dynamics. A long-term goal of the study of isomerization dynamics in molecules of this size would be to develop general rules connecting key features of the potential energy landscapes of the molecules (e.g., in terms of the structure or degree of complexity of the disconnectivity diagram) to the time scales, pathways, and product yields formed in the isomerization process.[30] New experimental tests of energy flow and vibrational mode specificity in the isomerization of large molecules also are needed,[31] because nonstatistical effects are predicted to increase in importance in large-molecule isomerization over small barriers.[18,32−36] Finally, the role that solvent plays in modifying the solute's potential energy landscape and conformational dynamics, or in creating new types of isomerization processes, needs to be assessed.

The presence of many conformational minima that are similar in energy raises the prospect that at typical experimental temperatures the Boltzmann distribution of population will be

spread over many conformations. For instance, even in tryptamine, the simplest molecule in our series, ab initio calculations predict that there are seven conformations with energies within 1 kcal/mol of the global minimum on the surface.[21] Any attempt to study the rates of isomerization between these minima or to identify key isomerization pathways is likely to fail in the absence of conformation-specific excitation and detection. Under such circumstances, it is highly desirable to develop experimental tools that are capable of dissecting the complex potential energy surface into smaller pieces associated with specific reactant-product isomer pairs.

Detection and Spectroscopy of Single Conformers. The primary subject of this review is recent advances in the conformation-specific and state-selective study of conformational isomerization dynamics in molecules with several flexible coordinates. However, a necessary prerequisite for studies that involve selective excitation and detection of single conformational isomers is the determination of the spectroscopic signatures for each of the isomers present.

Of the spectroscopic probes that can be used to characterize molecular conformation (e.g., NMR,[37,38] circular dichroism,[39] microwave,[40,41] Raman[42]), we will focus on infrared and ultraviolet spectroscopy, which serve as the basis for the dynamics studies reviewed here. Most of the molecules of biological relevance are polymers composed of amino acid or nucleic acid subunits. In peptides, the conformation of the peptide backbone can be probed via the absorptions of the amide groups in the backbone or of the various amino acid side chains. In the infrared, the amide groups possess strong chromophores (e.g., NH stretch, C═O stretch, NH bend) whose frequencies and intensities are sensitive to molecular conformation.[43] Both the NH stretch and the C═O stretch fundamentals respond in characteristic ways to the presence and strength of intramolecular or intermolecular H-bonds.[44] Furthermore, the relative orientation and proximity of the amide groups produce characteristic couplings between them.[45] Even more subtle conformational distinctions (e.g., interactions of the XH group with an aromatic π cloud) can also produce small but reproducible spectral shifts ($\sim$10 cm^{-1}).[46] In all these cases, however, the contributions to the spectrum from different conformations are superimposed on one another, making detailed spectroscopic characterization difficult.

Two-dimensional infrared methods address the spectral complexity accompanying the study of conformationally flexible molecules in room-temperature solution by subjecting the sample to sequences of IR pulses that produce signals arising from anharmonic coupling between the infrared chromophores (e.g., the C═O groups).[45,47−51] These off-diagonal features in the two-dimensional spectrum reflect the spatial proximity and relative orientation of the anharmonically coupled groups and can thereby be used as a diagnostic of conformation and as a means to uncover the presence of multiple conformations even when they overlap in the linear absorption spectrum.

The use of electronic spectroscopy to distinguish conformational isomers requires that the molecules of interest incorporate an ultraviolet chromophore that possesses sharp vibronic structure, such as an aromatic ring. Three of the twenty naturally occurring amino acids in proteins have aromatic side chains that meet this criterion (tryptophan, tyrosine, and phenylalanine). However, the electronic frequency shifts induced by changes in the peptide backbone conformation are typically quite small ($<$500 cm^{-1} in a 30 000 cm^{-1} transition), so that the absorption spectrum is not a good indicator of conformation in bulk solution. The emission wavelength and fluorescence lifetime of tryptophan are sufficiently sensitive to environment that they have served as convenient tags of tryptophan's local environment in the protein, providing indirect structural information.[52,53] The bases adenine, guanine, cytosine, and thymine that serve as building blocks for DNA and RNA are also aromatic molecules with well-known ultraviolet absorptions but very poor fluorescence quantum yields in solution.[54]

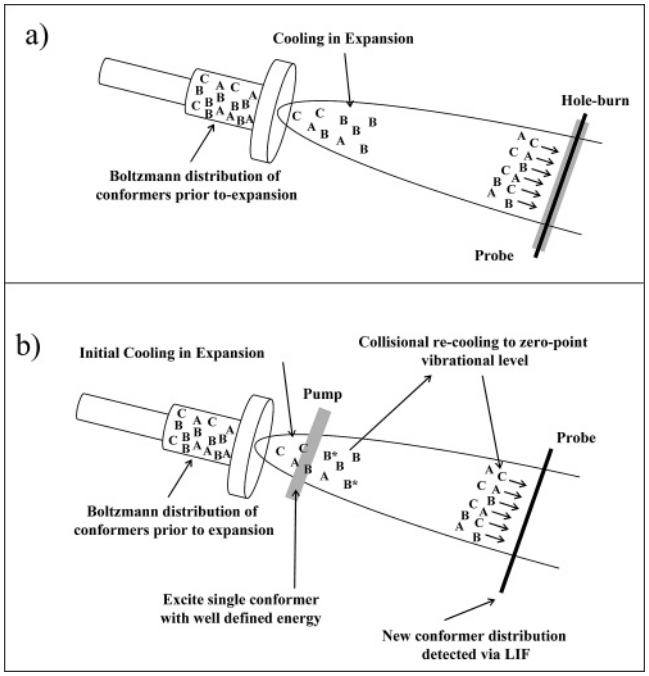

Figure 2. Schematic diagrams of (a) hole-burning conditions, in which both pump and probe lasers are in the collision-free region of the expansion, and (b) hole-filling conditions, in which the pump laser is positioned at a point where collisions can re-cool the laser-excited molecules back to the zero-point level(s) prior to detection with a probe laser downstream in the collision-free region.

An alternative route to conformation-specific spectral data is to seek more pristine conditions in which homogeneous and inhomogeneous broadening are minimized, and to combine those conditions with double-resonance spectroscopies that can dissect the spectrum into its contributions due to individual conformational isomers.[55−62] By studying the isolated molecules cooled in a supersonic expansion, it is possible to determine the conformational preferences of the isolated molecule, for comparison with those in solution. The efficient collisional cooling inherent to the expansion often traps conformational populations behind conformational barriers and cools these conformational populations to their respective zero-point levels. Typical rotational temperatures downstream in the expansion are $T_{rot} = 2-5$ K, leading to rotational band contours with widths of about 1 cm^{-1}. As a result, the IR and UV transitions due to different conformations are often resolved from one another.

Furthermore, because expansion cooling effectively quenches isomerization, hole-burning methods can be employed with great success. In hole-burning spectroscopy, a high-powered pump pulse burns a hole in the population of the zero-point level of a particular conformation via a strong infrared or vibronic transition out of that level. A delayed probe pulse in the ultraviolet can then detect this absorption as a decrease in the signal from the probe laser, as shown schematically in Figure 2a).

In UV−UV hole-burning spectroscopy, we find it best to fix the hole-burn laser and tune the probe laser, recording the difference in signal from the probe laser with or without the

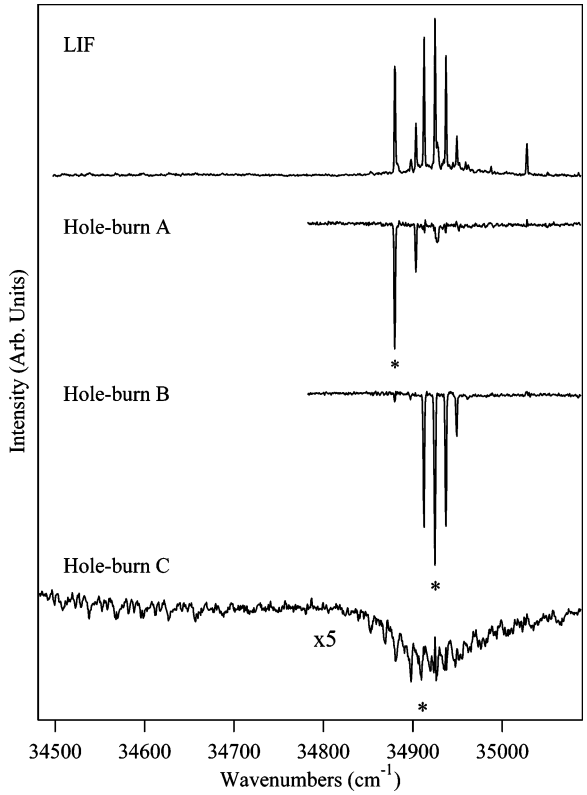

Figure 3. LIF spectrum and UV−UV hole-burning spectra of NATMA taken with the hole-burn laser fixed on the three wavelengths shown in the LIF spectrum with asterisks.

hole-burn laser present. The probe laser can be used to detect fluorescence (LIF) or, when mass selection is needed, resonant two-photon ionization (R2PI) time-of-flight mass spectroscopy can be employed. As an example, Figure 3 shows the LIF spectrum and UV−UV hole-burning spectra of NATMA, proving that there are three conformations with significant population that contribute to the LIF spectrum.[57]

The broad, congested ultraviolet spectrum of conformer C of NATMA is the result of a conformation-dependent shift in the excited states of the tryptophan chromophore.[63]

The infrared spectra of the individual conformations can be recorded in a similar way. In this case, the infrared hole-burn laser is tuned while the ground-state population of a given conformational isomer is monitored via LIF or R2PI. Figure 4 presents the fluorescence-dip infrared (FDIR) spectra of conformers A−C of NATMA in the NH stretch region.[57]

All low-energy conformations of NATMA share one of two conformations for the methyl-capped dipeptide backbone: an extended "C5" family that lacks intramolecular H-bonds and a $C7_{eq}$ family in which the amide NH from one amide group forms a H-bond with the C═O site of the adjacent amide subunit, forming a seven-membered H-bonded ring. It is obvious from the IR spectra of Figure 4 that isomers A and B belong to the C5 family, whereas conformer C is a $C7_{eq}$ structure, with an NH stretch fundamental that is shifted down in frequency to 3340 cm^{-1} due to the formation of an intramolecular H-bond. Specific conformational assignments for NATMA were made on the basis of the combined evidence from the infrared and ultraviolet spectra, utilizing the calculated vibrational frequencies and infrared intensities as points of comparison with the experimental results.

It should be noted that, even with the spectral simplification afforded by these double resonance methods under jet-cooled conditions, further spectral distinction is often desirable and has

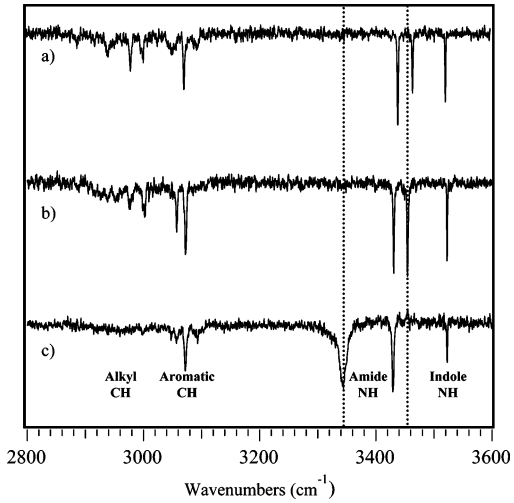

Figure 4. Fluorescence-dip infrared spectra of conformers A−C of NATMA over the 2800−3600 cm^{-1} region that includes the C−H and N−H hydride stretch fundamentals.

motivated continuing advances in the spectroscopy capabilities. Because the IR−UV double resonance methods rely on depletion for detection of the infrared absorption, the infrared source has to be of sufficient intensity to saturate or partially saturate the infrared transitions of interest. Until recently, these requirements imposed a long-wavelength cutoff of about 5 μm (2000 cm^{-1}) to the conformation-specific hole-burn spectra. However, several recent technical advances show promise for future studies that explore further into the complexity gap noted in the Introduction. First, free electron lasers such as FELIX are now providing conformation-specific spectra over the entire fingerprint region of the infrared.[64] Second, Gerhards and co-workers have recently demonstrated the use of a $AgGaSe_2$-based tabletop parametric converter to record IR−UV depletion spectra down to about 1000 cm^{-1}.[60,65] Third, Miller and co-workers have shown that it is possible to measure the vibrational transition moment directions of XH oscillators by aligning the molecular dipoles in a dc electric field and comparing the intensities of XH stretch fundamentals with infrared polarization parallel and perpendicular to the external field.[66] The angle between the infrared transition moment and the dipole moment provides a powerful additional diagnostic of the conformation responsible for the absorption. Finally, both thermal[60] and laser desorption methods[61,62,67−70] are now being used to record high-quality, conformation-specific spectra of larger molecules than ever before.

Before closing this section on conformation-specific spectroscopy, it is worth commenting briefly on the effect of the supersonic expansion on the conformational populations of these flexible, bioactive molecules. In all of the spectroscopy methods described in this section, the infrared and ultraviolet lasers are spatially overlapped with one another downstream in the expansion where cooling is complete and isomerization is quenched. To understand the relationship between the post-expansion conformational populations and their pre-expansion values, one needs to know much about the molecule and its potential energy surface, including the molecule's average internal energy prior to expansion, the rate of collisional cooling, the relative energies of the minima, and the heights of the barriers separating the minima. For the molecules of interest here, their average internal energy prior to expansion cooling (that is, at the temperature of the nozzle, T_{nozzle}) is several times the typical lowest energy barrier separating the minima. As a result, cooling occurs in parallel with isomerization. Isomer-

ization is quenched as the internal energy of the molecule falls below the lowest barrier to isomerization, E_{min}. In many circumstances, the preexpansion equilibrium and postexpansion populations will be quite similar to one another, particularly when the energy differences between minima are small relative to the barrier heights (so that $K_{eq}(T_{nozzle}) \sim K_{eq}(E_{min})$) or when cooling is fast compared isomerization. However, there are circumstances where cooling will selectively remove population from higher energy minima, making it difficult to associate the downstream populations with their upstream thermal populations in the absence of more detailed information about the potential energy surface. The dynamics studies described in the following sections touch on these issues further.

Protocol for Conformation-Specific Studies of Isomerization Dynamics. Armed with knowledge of the unique infrared and ultraviolet spectral signatures of the conformational isomers, we are prepared to address the primary subject of this article; namely, conformation-specific studies of isomerization dynamics for molecules with several flexible degrees of freedom. It is clear from the fluorescence-dip infrared spectra in Figure 4 that, with proper choice of infrared excitation frequency, it should be possible to selectively excite one conformational isomer in the mixture. For instance, if infrared excitation occurs at 3330 cm^{-1}, conformer C will absorb, whereas A and B will not. Similarly, infrared radiation at 3454 cm^{-1} will selectively excite B, but not A and C. In so doing, the excited conformer would acquire about 10 kcal/mol of additional internal energy that the other conformers do not possess. This energy is well above many of the lowest energy barriers to conformational isomerization (~3−5 kcal/mol), as shown in the disconnectivity diagram of Figure 1. Therefore, IR excitation of a single conformer can be used to initiate its conformational isomerization.

If infrared excitation was carried out in the collision-free region of the expansion, as occurs in the hole-burning methods (Figure 2a), these "hot", laser-excited molecules would have broad ultraviolet absorptions that lacked conformation specificity. However, by moving the excitation laser upstream to a position close to the expansion orifice (Figure 2b), laser excitation occurs in a collision-dominated region of the expansion where substantial cooling has already taken place, yet the laser-excited molecules will still undergo many collisions after excitation that re-cool them back to their zero-point levels prior to detection with the "downstream" probe laser. This experimental protocol is referred to as "hole-filling" conditions, because the hole created in the ground-state population by laser excitation is allowed to fill back in (if isomerization does not occur) or to increase the population of other isomers (if isomerization does occur).[71−73] When the population is re-cooled back into the zero-point levels of the isomers, the probe laser can detect the changes induced by the excitation laser in a conformation-specific fashion. The cool−pump−cool−probe scheme thus sacrifices direct knowledge of the isomerization process in the absence of collisions in favor of conformation-specific detection of the products formed. By detecting only the changes in population induced by the excitation laser(s), the hole-filling method is capable of studying each reactant−product pair free from interference from other isomerization processes that might be occurring at the same time. This provides a powerful scheme for dissecting an inherently complicated isomerization process involving many species into a series of studies of individual reactant−product isomer pairs. Furthermore, because laser excitation is carried out on molecules that have already been cooled to their zero-point levels (we measure $T_{vib} \sim 15$ K for NATMA at the point of excitation),[25] the conformer selected for excitation receives a well-defined amount of energy (known to within a few inverse centimeters) in initiating the isomerization process.

To date, two laser excitation schemes have been used in hole-filling studies: infrared excitation in the hydride stretch region of the infrared[25,71−73] and stimulated emission pumping.[21,74−77] Each has its own advantages and limitations. Infrared excitation requires a single infrared light source operating in the near-infrared, where high-powered lasers are available. These laser sources are capable of saturating hydride stretch fundamentals, moving up to 50% of the population in so doing. Because hole-filling methods rely on the observation of a change in population downstream in the expansion, moving substantial populations is a key to detection. To a good approximation, the XH stretch normal modes involve localized motion of a single bond in the molecule. If these XH stretch fundamentals have unique infrared frequencies, it is possible to initiate the isomerization of a given conformation in a mode-specific way via each of these XH stretch fundamentals. One can then probe whether such vibrationally mode-specific excitation has any effect on the isomerization product yield. A drawback of hydride stretch infrared excitation is that it gives to the excited isomer an amount of energy (~3500 cm^{-1} = ~10 kcal/mol) that is well above many of the lowest energy barriers to isomerization (~3−5 kcal/mol, Figure 1). As a result, hydride stretch infrared excitation typically does not directly probe the energy thresholds for isomerization. This drawback of infrared excitation may be removed soon, as the mid-infrared parametric conversion schemes mentioned earlier[65] are employed more generally for these studies.

When stimulated emission pumping is used as the vibrational excitation scheme, two independently tunable ultraviolet lasers replace the infrared source. The "pump" laser is fixed on a vibronic band (typically the S_0-S_1 origin transition) of the conformer to be selectively excited. A fraction of the excited population is then stimulated back down to a particular vibrational level in the ground state with a second ultraviolet laser (the "dump" laser) tuned to an $S_1(v') \rightarrow S_0(v'')$ transition. This dump step relies on good Franck−Condon factors in the $S_1(v') \rightarrow S_0(v'')$ transition for efficient population transfer. To be successful, the S_1 state must be long-lived enough to drive population from the S_1 state to $S_0(v)$ on a time scale that is short compared with the S_1 lifetime. As we shall see, many aromatic ultraviolet chromophores have good Franck−Condon factors spread over transitions to ground-state levels that stretch from well below to well above the lowest thresholds to isomerization.[21,74−77] This is the principle advantage of SEP over infrared excitation, because SEP can be used to directly probe the thresholds to isomerization. Furthermore, aromatics often have S_1 lifetimes in the nanosecond regime, sufficiently long-lived to carry out efficient SEP using high-powered, nanosecond lasers. SEP also has increased selectivity over infrared excitation, because the ultraviolet pump transitions have to differ from one conformer to another by only about 1 cm^{-1} out of 30 000 to enable selective excitation of a single conformer. The principle disadvantage of SEP relative to infrared is the increased complexity of the experimental setup, which now employs three independently tunable lasers, rather than two when infrared excitation is employed. In addition, the maximum fractional population that can be moved from the zero-point level to a vibrationally excited ground-state level is somewhat less using SEP (~25%) than using infrared excitation (~50%).

Infrared-Induced Conformational Isomerization

The first studies employing the hole-filling experimental protocol involved infrared-induced isomerization of *N*-acetyltryptophan amide (NATA), *N*-acetyltryptophan methyl amide (NATMA),[72] and melatonin.[73] The unique infrared signatures of NATMA and NATA[57] triggered our interest in pursuing conformation-selective isomerization dynamics studies using the amide NH stretch fundamentals. Melatonin (5-methoxy-*N*-acetyltryptamine) is an interesting test case, because it possesses both *trans*-amide (conformers A−C) and *cis*-amide (conformers D and E) conformers that are separated from one another by a large barrier of about 15−20 kcal/mol.[78] The results from the studies of these three molecules will be used to illustrate the types of information that can be gleaned from conformation-specific studies of the isomerization dynamics using hole-filling methods.

Conformation-Specific Quantum Yields in the Frequency Domain. Two types of spectra can be recorded using the hole-filling protocol, depending on whether the IR excitation or the UV probe laser is tuned. In IR−UV hole-filling spectroscopy, the infrared laser is held fixed at a wavelength where selective infrared excitation of a single conformation is possible. The ultraviolet laser is then tuned through the transitions of interest in the LIF spectrum. To highlight the effects of the infrared laser on the downstream populations, the difference in LIF signal is recorded by pulsing the IR laser every other time the UV laser fires, and recording the difference signal using active baseline subtraction.[73] In this way, dips in population are seen as depletions in the LIF spectrum, whereas gains in population will produce positive-going signals. As a result, IR−UV hole-filling spectroscopy can be used to determine where the population went following infrared excitation of a single conformer.

To illustrate, Figure 5 presents the LIF spectrum of melatonin (Figure 5a) and compares it with two IR−UV hole-filling spectra (Figure 5b,c) following conformation-selective excitation of conformers A and B with the infrared laser, respectively.[73] When conformer A is selectively excited at 3480 cm^{-1} (Figure 5b), its population downstream in the expansion is decreased, leading to a dip in the LIF signal from the S_0-S_1 origin of conformer A. At the same time, the signals due to conformers B and C show clear gains, indicating that the population lost in conformer A has undergone isomerization to form B and C. Alternatively, when B is excited at 3495 cm^{-1} (Figure 5c), the transitions due to B decrease, while those from A and C increase. These spectra illustrate several distinguishing features of the method. First, the method is capable of efficient and conformation-selective isomerization, as anticipated. Large fractional changes in population can be induced with the infrared laser following selective excitation of a single conformer in a well-defined NH stretch oscillator. Second, despite the fast cooling, there is no evidence for the IR-induced formation of new isomers. Instead, the infrared excitation moves population between the isomers that had the population in the absence of infrared excitation. We had hoped that the combination of selective excitation and fast cooling might trap population in conformational wells that had no population in the absence of the infrared, but to date this has not been observed. Third, the method demonstrates a degree of control over the downstream population that moves beyond merely taking what nature provides on its own in the supersonic expansion process. Simply by choice of the infrared wavelength, one can change the conformational populations downstream in the expansion, pushing the distribution toward certain isomeric products at the expense of others. Finally, the

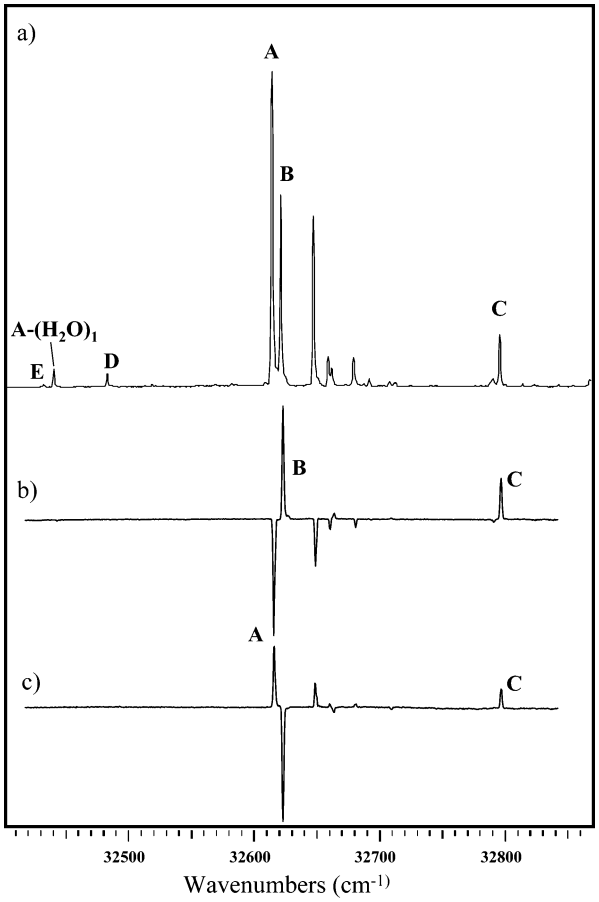

Figure 5. (a) LIF spectrum of melatonin and (b), (c) IR−UV hole-filling spectra following conformation-selective excitation of conformers A and B with the infrared laser, respectively. [Reproduced from ref 74, with permission. Copyright 2004 AAAS.]

population can only be moved within conformational subspaces that are energetically accessible to one another at the excitation energy used (~3500 cm^{-1} = 10 kcal/mol). No increase in the population of the *cis*-amide conformers of melatonin (D and E) is observed when any of the *trans*-amide conformers of melatonin are excited in the infrared (A−C).[73] This is a direct consequence of the high barrier to cis−trans isomerization of an amide group (15−20 kcal/mol).[78] In such circumstances, the hole-filling methods only explore isomerization within the *trans*-amide conformational subspace.

The alternative laser tuning scheme, in which the ultraviolet probe laser is fixed and the (upstream) IR laser is tuned, is called IR-induced population transfer spectroscopy (IR−PTS), because it detects the population changes induced in a single conformer by infrared excitation. As it turns out, this form is the more useful of the two for extracting quantitative data on the isomerization process. In IR−PTS, the UV laser is fixed on a vibronic transition in the LIF spectrum ascribable to a particular conformer. The magnitude of the LIF signal is directly proportional to the ground-state population of that conformer in its zero-point level. As the infrared source is tuned, infrared transitions due to that conformer show up as depletions in the LIF signal, whereas transitions that pump population out of other conformations into the one probed will lead to gains in signal. With proper normalization, these can be plotted as fractional changes in population of the product conformer as a function of infrared excitation frequency.

Figure 6 presents an overlay of three IR−PT spectra in the amide NH stretch region of the infrared with selective monitor-

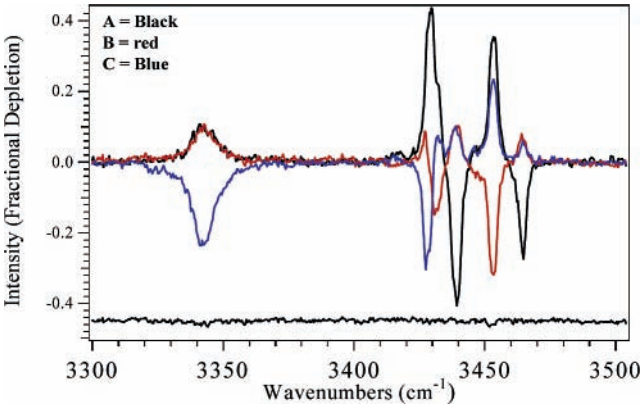

Figure 6. Overlay of three IR-population transfer spectra taken while monitoring the downstream populations of each of the three conformational isomers of NATMA. Positive (negative) signals indicate a gain (loss) in population of the detected conformer at that wavelength. The lower trace is a weighted sum of the three above it, with weighting factors $F_A = 0.20$, $F_B = 0.50$, and $F_C = 0.20$, demonstrating the null condition embodied in eq 2 of the text.

ing of the populations of each of the three conformational isomers of NATMA.[72]

By overlaying these spectra, it is easy to observe the "reflection symmetry" of the spectra, in which dips (population loss) in one IR−PT spectrum are compensated by corresponding gains in the other IR−PT spectra. In fact, if these spectra are recorded under identical conditions, they can be used to check quantitatively that there is no net loss of population in the IR-induced isomerization process; that is, at all infrared frequencies,

$$\Delta N_{tot}^{dn}(\tilde{\nu}) = \Delta N_A^{dn}(\tilde{\nu}) + \Delta N_B^{dn}(\tilde{\nu}) + \Delta N_C^{dn}(\tilde{\nu}) = 0 \quad (1)$$

Because the population transfer spectra each represent the fractional change in population of the monitored conformer, a weighted sum of the population transfer spectra in which the weighting factors are the fractional abundances (F_J) should properly add to zero at all infrared wavelengths:

$$F_A^{dn} \cdot I_A^{PT}(\tilde{\nu}) + F_B^{dn} \cdot I_B^{PT}(\tilde{\nu}) + F_C^{dn} \cdot I_C^{PT}(\tilde{\nu}) = 0 \quad (2)$$

This is demonstrated in the lower trace of Figure 6 for NATMA where such a weighted sum is plotted for $F_A = 0.20$, $F_B = 0.50$, and $F_C = 0.30$. Thus, IR−PT spectroscopy can be used to directly measure the fractional abundances of the conformational isomers in the expansion. However, one must be aware of the fact that these fractional abundances only are relevant to the conformational subspace between which isomerization can occur following infrared excitation in the relevant wavelength range. For instance, the corresponding measurements in melatonin only determined the fractional abundances of the *trans*-amide conformers but provides no way to relate those fractional abundances to the corresponding measurements for the *cis*-amide conformers, because the barrier to cis−trans isomerization is well above the 10 kcal/mol energy placed in the molecules by NH stretch infrared excitation.

The set of population transfer spectra can also be used to extract conformational isomerization product quantum yields following selective excitation of the hydride stretch fundamentals of each conformational isomer.[25,72] To do so requires the set of population transfer spectra to be combined with a measure of the fractional population excited by the infrared. This latter quantity is determined by recording a set of "warm FDIR" spectra in which the UV is overlapped with the infrared in the upstream position, recorded with insufficient time delay between

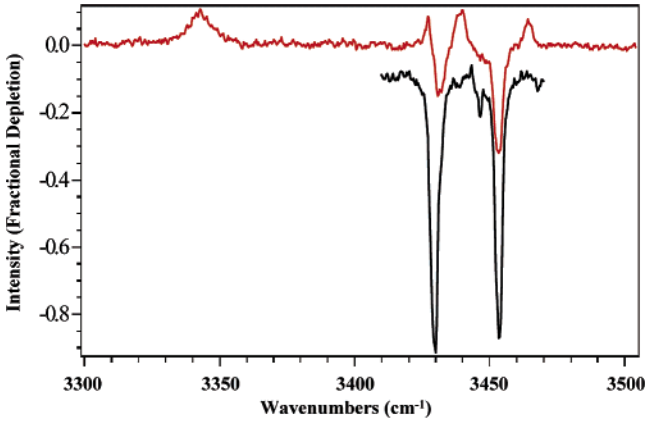

Figure 7. Comparison of the "warm FDIR" spectrum (lower trace in black) and IR−PT spectrum (upper trace in red) of conformer B of NATMA. The warm FDIR spectrum was taken with the IR and UV overlapped upstream in the expansion, with short delay so that no hole-filling can occur. Note that refilling of the zero-point level rotational population on the time scale of the nanosecond laser pulse can create large fractional depletions in the warm FDIR spectrum. The IR−PT spectrum has the UV probe laser downstream where collisional cooling of the laser-excited molecules back to the zero-point level is complete.

IR and UV laser pulses for the molecules to cool back to the zero-point level. Figure 7 compares the warm FDIR and IR−PT spectra of conformer B of NATMA, showing the large dips characteristic of the warm FDIR spectra, and the smaller depletions in these same regions characteristic of the IR−PT conditions in which part of the excited population fills back into the IR-created hole in the reactant population.

At wavelengths where another conformer (e.g., conformer A) is selectively excited by the infrared, the gain in signal in the PT spectrum reflects an increase in population of conformer B as the result of isomerization from A into B. The details of the fitting method for extracting quantitative quantum yields and for placing error bars on the quantum yields are given elsewhere.[72]

To date, we have recorded full data sets for NATMA, NATA, and the *trans*-amide conformers of melatonin.[25,72,73] Figure 8 provides a pictorial summary of the product quantum yields for NATMA (Figure 8a) and melatonin (Figure 8b) using triangle plots analogous to those used in ternary phase diagrams. In such a plot, the set of product quantum yields constitutes a single point on the diagram, with 1σ error bars displayed as areas on the plot. The dark circles on each plot are the fractional abundances of the isomers in the absence of the infrared.

The results in Figure 8 highlight several general features of the conformational isomerization dynamics in molecules of this size. In all cases, the product quantum yields favor the same conformers that carry the bulk of the population in the absence of the infrared. This is not surprising, because in the limit that vibrational cooling is slow compared to isomerization, one would anticipate an equilibration of the conformer population at the energy E_{vib} that should be qualitatively similar to the thermal Boltzmann distribution. Evans et al. have modeled the NATMA hole-filling experiment using a master equation kinetics approach built on RRKM rate constants.[25] As a function of vibrational cooling rate, the product quantum yields move smoothly from equilibrium populations (slow cooling) to the point where isomerization is effectively quenched (fast cooling). Using an experimental estimate of the vibrational cooling rate, the model predicted that the quantum yields should be somewhere between these extremes, with quantum yields that bore some resemblance to the equilibrium populations but are

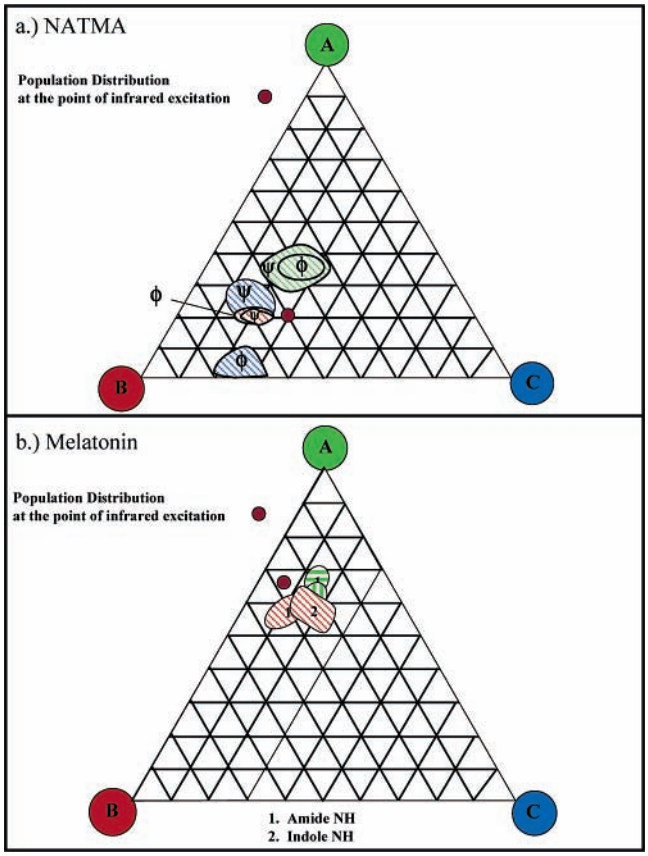

Figure 8. Product quantum yield triangle plots for (a) NATMA and (b) melatonin, following selective excitation of the indicated NH stretch fundamental of each conformational isomer of the molecule. The inscribed areas in the plots represent one-standard deviation on the mean. The brown dots indicate the fractional abundances of the molecules in the absence of the infrared excitation, determined from the null weighted sum in eq 2. It was not possible to obtain accurate product yield data following excitation of conformer C of melatonin (ref 78).

modified by the fact that cooling occurs on the same time scale as isomerization. This prediction is consistent with observation, where the product yields are similar, but not identical, to the distribution in the absence of the infrared.

The differences in quantum yields among the various conformation-specific infrared bands are somewhat larger in NATMA than in melatonin, consistent with the greater size and flexibility of NATMA. The theoretical modeling of Evans et al. gives insight to the time scale for isomerization and the degree of complexity of the isomerization pathways involved.[25] Using the potential energy surface depicted in the disconnectivity graph of Figure 1, microcanonical RRKM rate constants were computed for the various isomerization steps. With these rates in hand, it is possible to describe the kinetics of the system using a master equation approach. The rate of change of occupation probability P_i of minimum i is given by

$$\frac{dP_i(t)}{dt} = \sum_{j \neq i} [k_{ij}(E)\, P_j(t) - k_{ij}(E)\, P_i(t)] \qquad (3)$$

These equations were integrated numerically as a function of time, updating the rate constants $k_{ij}(E)$ as the energy changes via the cooling collisions. Experimental data on the time scales for the population arriving at the zero-point levels of the various minima were used to estimate the experimentally relevant collisional cooling rate. By looking at the population fluxes as a function of time, it was determined that the dominant isomerization pathways connecting minima A, B, and C involve multistep, competing pathways that sample about 10 minima.[25] At an initial internal energy of 10 kcal/mol internal energy, isomerization was largely complete on the 1 ns time scale, with all final populations frozen in on the tens of nanoseconds time scale. The model correctly predicted that, on these time scales, some degree of conformation selectivity to the product yields would occur in NATMA, as observed experimentally.

There is also a hint of vibrational mode specificity in the data for NATMA, whereas none is evident in the data for melatonin. In NATMA, the product quantum yields of the two amide NH stretch fundamentals of conformer C are clearly outside the 1σ error bars. This magnitude of difference is not sufficient to prove mode specificity in NATMA. Nevertheless, it is intriguing to note that this hint of mode specificity occurred in conformer C, the intramolecularly H-bonded conformer of NATMA (Figure 4), in which one of the NH groups is involved in a H-bond, and the other is not. These different environments for the two amide NH bonds could affect the rate of IVR out of the NH(υ=1) level and within the first tiers of levels to which it is most strongly coupled, which could in turn lead to mode-specific quantum yields. Further work on molecules covering a wider range of sizes and potential energy landscapes is clearly warranted to explore such effects further.

The isomerization quantum yields in melatonin (small conformation specificity and no mode specificity) appear to be nearer the "slow cooling" limit of product equilibration than those for NATMA (small mode specificity and somewhat more distinct conformation specificity). A quantitative accounting of these differences awaits a detailed characterization of the melatonin potential energy surface. At present, we can only put forward qualitative arguments that motivate future work involving molecules with a wider range of sizes and conformational complexity.

Melatonin is only slightly smaller in size than NATMA (by three atoms) but trades a simpler flexible side chain (with a single amide group in the 3-position on indole) for the presence of a second side chain (methoxy) in the 5-position. Notably, preliminary searches of the potential energy surface of melatonin indicate that the rate-limiting barriers separating the low lying minima were 3−4 kcal/mol rather than the 5−7 kcal/mol found for NATMA.[25,73] This suggests that the ethylacetamido group is less constrained in melatonin than the methyl-capped dipeptide in NATMA. Smaller barriers to isomerization in melatonin should lead to faster isomerization rates in melatonin than in NATMA at the same energy of excitation. In addition, the less complex potential surface should lead to shorter pathways between the low-lying minima. Both these features should result in faster equilibration between the conformational isomers in melatonin than in NATMA, consistent with the quantum yield results.

Conformation-Specific Quantum Yields in the Time Domain: Melatonin and 5-Methoxy-NATMA. One of the predictions made by the theoretical modeling of isomerization in NATMA[25] was that the combination of conformation-specific excitation and fast cooling could lead to trapping of population in previously unpopulated conformational minima along the isomerization pathway. This possibility was one of the original motivations for this work; namely, to use laser excitation combined with fast cooling to trap population in new conformational minima not observed in the absence of laser excitation. Favorable conditions are those in which cooling occurred on a

time scale competitive with isomerization, where the quenched product quantum yields are far from equilibrium.

Motivated by the modeling results, we have explored experimental conditions where vibrational cooling on the nanosecond time scale can be achieved. 5-methoxy-NATMA

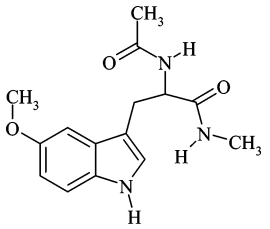

5-methoxy-NATMA

is a close analogue of NATMA, differing only in the addition of a methoxy substituent in the 5-position on the indole ring.[73] Despite this similarity, 5-methoxy-NATMA funnels all of its population into a single C5 conformer under expansion cooling. A comparison of the calculated energies of the low-lying conformers of NATMA and 5-methoxy-NATMA suggests that the 5-methoxy substituent destabilizes conformers in which the flexible side chain interacts with the phenyl ring of indole. Because all the population of 5-methoxy-NATMA exists in a single conformer, vibrational relaxation can be studied in the absence of isomerization. With a high backing pressure expansion and large nozzle diameter, it is possible to remove the entire 3500 cm^{-1} of energy gained from laser excitation within 50 ns by collisions with helium. Even greater cooling rates might be anticipated for other collider gases (e.g., Ne or Ar); however, extensive cluster formation with Ne or Ar kept us from exploring the same high-pressure conditions.

The fast cooling conditions achieved in the high-pressure helium expansion open the way for hole-filling studies of conformational isomerization in the time-domain.[73] When the IR and UV laser beams are overlapped in the high density region of the expansion, the population changes induced by selective infrared excitation could be studied simply by varying the time-delay between the two lasers. Figure 9 presents a series of such scans following selective IR excitation of conformer B of melatonin.

These time-domain traces show depletion in conformer B population at short times that is matched by a corresponding increase in the populations of conformers A and C. Once vibrational cooling is complete, the time-domain analogue of eq 2 can be used to extract fractional abundances for the conformer populations.

$$F_A^{dn} \cdot I_A^{PT}(t) + F_B \cdot I_B^{PT}(t) + F_C \cdot I_C^{PT}(t) = 0 \qquad (4)$$

At early times, this weighted sum is not zero, because the population has not cooled back to the zero-point levels of reactant and product. However, the weighted sum does return to zero on the 50−100 ns time scale, as anticipated on the basis of the cooling data on 5-methoxy-NATMA. More importantly, product quantum yields can also be determined from the time-domain scans.

The data in Figure 9 were used to determine product quantum yields under these fast-cooling conditions. To extract product quantum yields, it is necessary to know the effect of movement of the IR-excited molecules out of the region of spatial overlap with the probe laser beam due to the velocity of the expansion. This was accomplished by viewing the time-dependent signal of the excited conformer in the absence of re-filling collisions

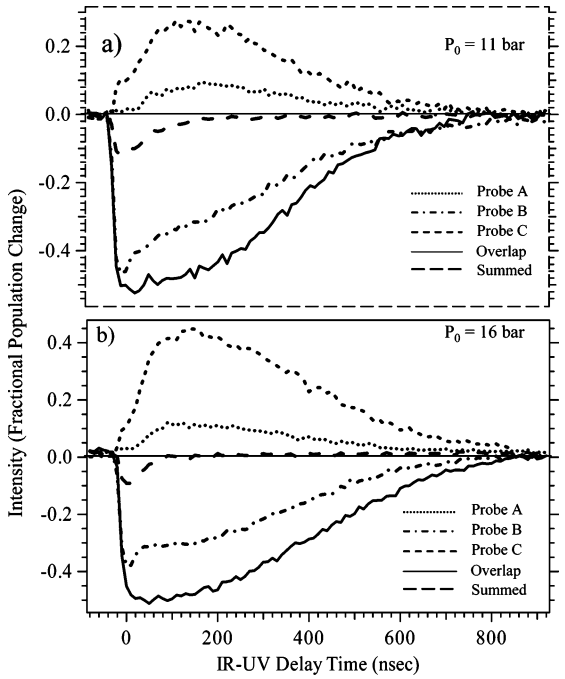

Figure 9. Time-dependent population changes following selective IR excitation of conformer B of melatonin at 3495 cm^{-1}. All conditions of the scans in (a) and (b) were identical, except for the change in helium backing pressure (11 bar vs 16 bar, respectively).

(the solid line in Figure 9). The details of extracting quantum yields from the time-domain scans are given elsewhere.[73] The striking result of these studies, evident in the raw data of Figure 9, is that the yield of conformer C is increased by almost a factor of 2 as the backing pressure is raised from 11 (Figure 9a) to 16 bar (Figure 9b). This indicated that collisional cooling was competing with isomerization and suggests that conformer C may be an intermediate along the pathway from B to A that gains population as faster cooling occurs.

In summary, the fast cooling results for melatonin, like the standard cooling results on NATMA, show that isomerization and cooling are occurring on similar time scales so that the product yields can be tuned by varying the rate of cooling. If similar studies that utilize selective infrared excitation can be extended to molecules of somewhat greater size and flexibility, the methods described here may uncover more dramatic conformation-specific and mode-specific effects. In larger flexible molecules, it seems likely that the rates of isomerization will slow relative to vibrational relaxation, thereby moving the observed product yields further from their equilibrium values.

SEP−Based Studies of Conformational Isomerization

One of the principle drawbacks of the infrared studies just discussed is that near-infrared excitation in the hydride stretch fundamental region (2800−3800 cm^{-1}) places 8−11 kcal/mol of energy into the conformation of interest, an amount well in excess of the typical lowest energy barriers to isomerization. In favorable cases, with SEP excitation it is possible to tune the internal energy of the excited conformation over a much wider range, stretching from below to well above the lowest energy barriers to isomerization. As a result, one can use SEP hole-filling studies to determine the energy thresholds for isomerization for individual X → Y reactant−product pairs. Furthermore, the access that SEP excitation gives to the threshold region also means that the rates of isomerization and the time scale for collisional quenching of isomerization can

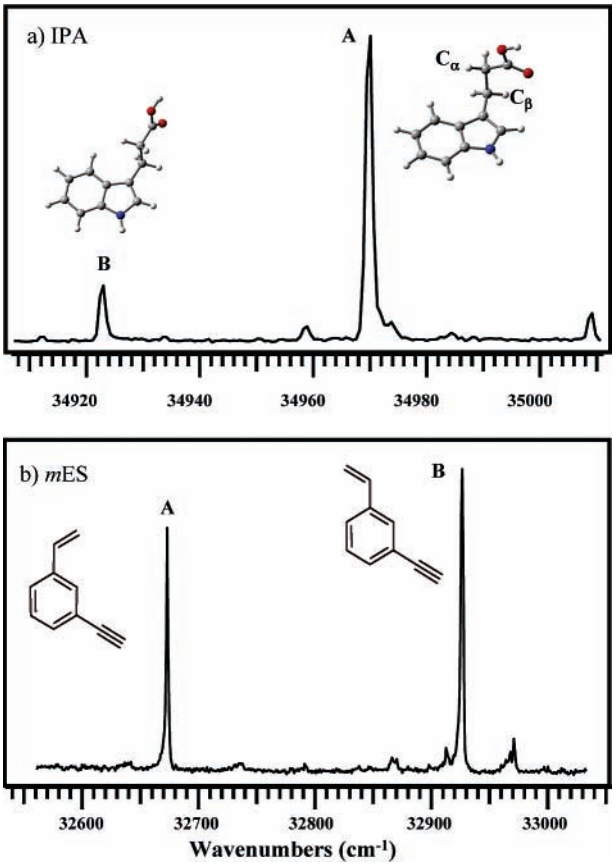

Figure 10. $S_1 \leftarrow S_0$ origin transitions of the two indicated conformers of (a) 3-indolepropionic acid (IPA) and (b) *meta*-ethynylstyrene.

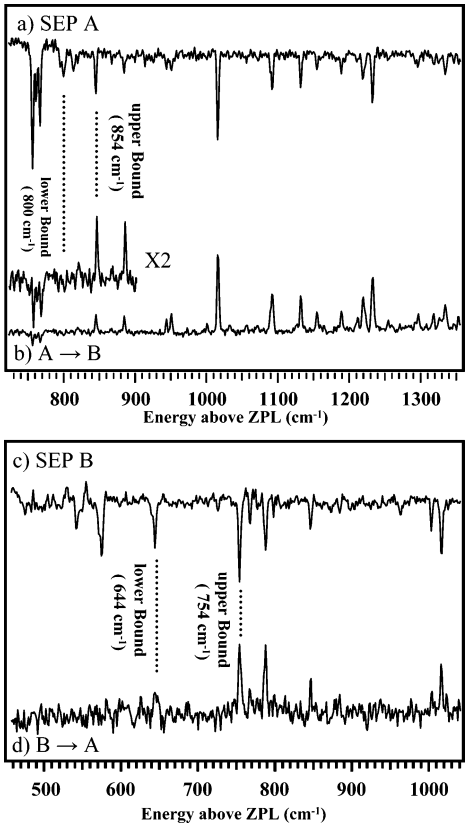

Figure 11. (a), (c) SEP spectra of conformers A and B of IPA. (b), (d) SEP−PTS for the (b) A → B and (d) B → A reactant−product pairs. The abscissa in these plots is the internal energy of the IPA conformer (in cm^{-1}) produced in the dump step.

be tuned over wide ranges in searching for conformation-specific or vibrationally mode-specific effects.

Isomerization Involving Two Conformers: 3-Indolepropionic Acid and *meta*-Ethynylstyrene. Of the molecules studied to date, 3-indolepropionic acid (IPA)[75] and *meta*-ethynylstyrene (*m*ES)[77] are particularly instructive first examples, because they both possess just two conformational isomers with measurable population. As a result, SEP population transfer spectroscopy can be used to measure the energy thresholds for isomerization involving only two reactant-product pairs: A → B and B → A. Because these two measurements probe the same rate-limiting barrier from either direction, the difference in the observed threshold energies constrains the relative energies of the two minima, A and B:

$$E(\mathrm{B}) - E(\mathrm{A}) = \Delta E_{\mathrm{min}} = E_{\mathrm{barrier}}(\mathrm{A}\rightarrow\mathrm{B}) - E_{\mathrm{barrier}}(\mathrm{B}\rightarrow\mathrm{A})$$
$$= [E_{\mathrm{thresh}}(\mathrm{A}\rightarrow\mathrm{B}) - E(\mathrm{A})] - [E_{\mathrm{thresh}}(\mathrm{B}\rightarrow\mathrm{A}) - E(\mathrm{B})] \quad (5)$$

Furthermore, in both IPA and *m*ES, the conformers can interconvert along a well-defined coordinate, involving hindered rotation about the C(α)-C(*β*) bond in IPA (Figure 10a) and the out-of-plane torsion of the vinyl group in *m*ES (Figure 10b). The $S_1 \leftarrow S_0$ origin transitions of these isomers are shown in the R2PI spectra in Figure 10. These transitions are used as pump transitions in SEP to selectively excite one or the other conformer.

The SEP spectra for conformers A and B of IPA (Figure 11a,c) and *m*ES (Figure 12a,c) show strong dump transitions spread over the range from 500 to 1300 cm^{-1}. Rather than plotting the abscissa as a wavelength range for the dump laser, the difference in photon energy (in cm^{-1}) between the pump and dump lasers is displayed to show directly the energy given to the excited conformer by the SEP steps. The spectral range shown in each case encompasses the threshold region of interest for each conformer pair.

The population transfer spectrum depicted in Figure 11b measures the gain in the downstream population of conformer B of IPA following excitation of A upstream. Below the barrier to isomerization, no population can be transferred between A and B, and the SEP dump step produces no change in the LIF signal from B. The first observed transition in the A → B SEP−PT spectrum (at 854 cm^{-1}) measures the threshold energy for IPA(A) → IPA(B) isomerization. As long as tunneling is not significant, this threshold energy places a firm upper bound on the energy barrier to A → B isomerization. Because the isomerization involves motion of the entire COOH group between gauche and anti positions relative to the ring, we do not anticipate tunneling to be significant.

The dotted line at 800 cm^{-1} in Figure 11b marks the last transition in the PT spectrum that should have been observable on the basis of the intensity of the transition in the SEP spectrum above it. Inherent to the hole-filling experimental protocol is a competition between isomerization and collisional cooling of the laser-excited molecules. The general kinetic expression contained in eq 3 simplifies to just two terms in the present case in which isomerization occurs between only two minima. A modified form of this expression can be used to evaluate the intensity of transitions in A → B SEP population transfer spectra of IPA and *m*ES. If $A(t_0)$ is the initial concentration of conformer A produced by the SEP dump step with energy E_0, then the

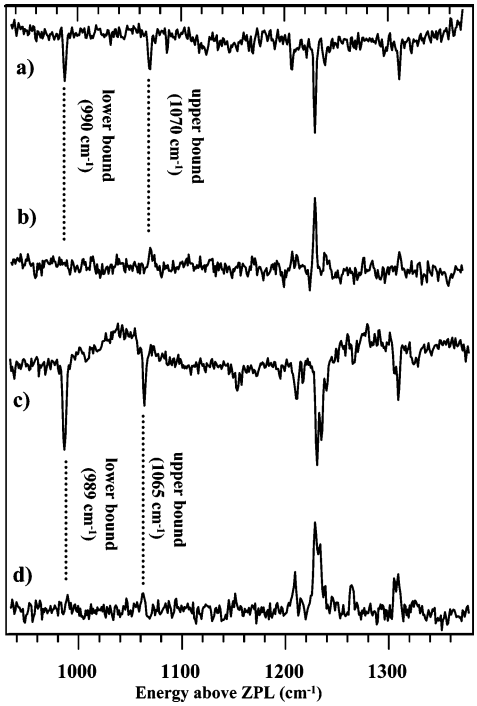

Figure 12. (a), (c): SEP spectra of the cis (A) and trans (B) conformers of *meta*-ethynylstyrene. (b), (d) SEP−PTS for the (b) cis → trans and (d) trans → cis reactant−product pairs.

population change induced in conformer B by the dump laser is

$$B(t_{\text{final}}) = \sum_{n=0}^{n_{\text{tot}}} [k_{A\rightarrow B}(E_0 - n\cdot\Delta E)\cdot A(t_n) - k_{B\rightarrow A}(E_0 - n\cdot\Delta E)\cdot B(t_n)]\cdot\Delta t \quad (6)$$

where $k_A \rightarrow B(E-n\cdot\Delta E)$ is the rate constant for A → B isomerization at energy $E_0 - n\cdot\Delta E$, the sum is over n_{tot} collisions with helium, each of which removes an average energy ΔE, and t_n is the time of the nth collision, $t_n = t_0 + n\cdot\Delta t$ where $\Delta t = 1/z_{jet}$ is the time between collisions with helium at the point of SEP excitation in the jet. The total number of collisions with helium n_{tot} is determined by the amount of energy needed to remove the excess energy down to the A → B isomerization threshold (where further isomerization is quenched).

When isomerization is fast compared to vibrational cooling, equilibrium is established, in which the rates of forward and backward reaction are equalized before the threshold energy is reached. In such circumstances, $B(t_{final})$ is under thermodynamic control, with a magnitude determined by the amount of A excited in the SEP step and the equilibrium constant at the threshold internal energy, $K_{eq}(E_{thresh})$:

$$B(t_{\text{final}}) = K_{eq}(E_{\text{thresh}})\cdot[A(t_0) - B(t_{\text{final}})] = K_{eq}(E_{\text{thresh}})\cdot A(t_{\text{final}})$$

$$B(t_{\text{final}}) = \left(\frac{K_{eq}(E_{\text{thresh}})}{1 + K_{eq}(E_{\text{thresh}})}\right)\cdot A(t_0) \quad (7)$$

In this limit, the intensities of transitions in the A → B population transfer spectrum will scale with their counterparts in the SEP spectrum of the reactant, conformer A in this case. The intensities in the A → B PT spectrum of IPA seem to fall in this limit, faithfully reflecting the relative intensities in the SEP spectrum beginning at the first observed transition at 854 cm^{-1}. Furthermore, the sharp turn-on at threshold, with no measurable intensity in transitions only a little below it in energy, argues for the last unobserved transition (at 800 cm^{-1}) lacking intensity because it places too little energy into IPA(A) for it to isomerize to B; that is, the last unobserved transition places a lower bound on the barrier to A → B isomerization in IPA.

This capability of PT spectroscopy to place direct experimental bounds on the barriers to isomerization between specific X → Y reactant-product conformer pairs is one of the most powerful attributes of the method. Spectroscopy typically focuses attention on the minima in the potential energy surface, characterizing their structures and the bound energy levels in these wells. By contrast, PT spectroscopy can be used to measure barrier heights, which are crucial for understanding the isomerization pathway and kinetics. In cases where the primary goal is to measure barrier heights, collisional conditions should be sought that are as slow as possible while still being sufficient to return the excited population back to the zero-point level before interrogation with the probe laser downstream. Whether such conditions can be achieved experimentally depends on the relative rates of isomerization and vibrational cooling.

In the opposite limit in which the collisional cooling rate is fast compared to isomerization, the yield of the product B would be under kinetic control:

$$B(t_{\text{final}}) = \sum_{n=0}^{n_{\text{tot}}} k_{A\rightarrow B}(E_0 - n\cdot\Delta E)\cdot A(t_n)\cdot\Delta t \quad (8)$$

In this limit, the intensities of transitions in the A → B PT spectrum are determined not only by the SEP intensity (which determines $A(t_0)$) but also by the rate constant for isomerization and the time to quenching $t_{quench} = n_{tot}\cdot\Delta t$. The transition intensities will be reduced from their equilibrium values, with magnitudes that depend on the cooling conditions used (the position of excitation and the backing pressure of the expansion). If isomerization is too slow at the threshold, the amount of B formed will be too small to be observed, producing a kinetic shift in the threshold. If the last unobserved transition were so by virtue of such a kinetic shift, it could not serve as a lower bound to the energy barrier to isomerization.

Both IPA and *m*ES show some evidence for threshold effects. The first observed band in the IPA A → B PT spectrum (Figure 11b) increases in intensity as the position of SEP excitation is moved downstream in the expansion (not shown), approaching its full SEP intensity under the slowest cooling conditions.[80] Similarly, in *m*ES, both the cis → trans and trans → cis PT spectra (Figure 12b,d) show first observed transitions at 1070 and 1065 cm^{-1} that are very weak relative to their intensities in the SEP spectra (Figure 12a,c) but are definitely present and reproducible. These peaks are reduced in intensity by the competition with vibrational cooling.

To evaluate whether isomerization in a given molecule falls nearer the fast or slow cooling limits at threshold, it is necessary to estimate the energy-dependent rate constant for isomerization and the collisional cooling rate. Accurate measurements of both quantities are lacking in molecules of this size (at least in these energy regimes near threshold). This motivates systematic studies of the intensities of bands near threshold as a function of cooling rate, a task reserved for future work. In the absence of such studies, one can estimate the isomerization rate constant using RRKM theory.[75,77] Such RRKM estimates are summarized for the systems studied so far in Table 1. By comparison, the vibrational cooling rate can be estimated on the basis of the extensive literature on vibrational cooling,[79−82] which indicates

TABLE 1: Experimental Energy Thresholds and Calculated Energy Barriers to Conformational Isomerization, and RRKM Estimates of Threshold Isomerization Rates

	thresholds (cm−1)		RRKM
	exptl	calcd	estimates[a] (s^{-1})
TRA (A → B)	688−748	929	2.2E9 (800)
c-*m*ES → *t*−*m*ES	990−1070	1237	2.6E9 (1000)
IPA(A → B)	800−854	750	1.1E8 (830)
IPA−H_2O (A → B)	771−830	780	1.9E7 (830)
TFA−H_2O (NH → C═O)	750−988	1110	2.3E7 (1000)

[a] Based on a harmonic density of states calculation at the indicated threshold energy, given in parentheses in cm^{-1}.

that, once the density of states has reached a quasi-continuum, the fractional energy lost per collision is approximately constant; that is, $\Delta E/E = \lambda$, where λ = a constant. On the basis of the studies of vibrational relaxation in NATMA and related molecules, a $\lambda \sim 0.003$ was chosen for numerical simulations conducted as a part of that work.[25,72,73] If the molecules in Table 1 have similar λ values, each collision with helium would remove about 3 cm^{-1} per collision at 1000 cm^{-1} internal energy, at a typical collision rate at the point of laser excitation of $z_{jet} = (1-5) \times 10^9$ s^{-1}.

The estimated rates in Table 1 cover over 2 orders-of-magnitude, indicating that the competition between isomerization and cooling can be studied over a wide dynamic range depending on the choice of system and amount of excess internal energy. In IPA and *m*ES, the estimated threshold isomerization rates are similar to the collision rate. The observation of reduced intensities in the first observed transitions in IPA and *m*ES suggests, then, either that these first transitions are to levels right at the barrier height or that the threshold isomerization rate is slower than that predicted by RRKM. The rate is predicted to rise quickly with energy above threshold so that the equilibration limit is quickly reached, consistent with the population transfer intensities following those in the SEP spectrum above the threshold energy. It is hoped that systematic studies will soon test whether RRKM theory can provide accurate predictions of isomerization rates in large molecules near threshold, a topic of current discussion.[19,31−33,83−85]

One final note before leaving these simple two-isomer examples. The astute reader will note that the above discussion has treated the collisions with the expansion seed gas as having no effect beyond removing internal energy from the conformational isomers. However, these collisions could also serve as a means of energy scrambling in the molecule, which could in principle actively redirect the products formed. Although our intuition is that such collisional effects on the product distributions will typically be small, the hole-filling methods cannot strictly speaking distinguish intramolecular from collision-induced effects, and the latter could be important in certain circumstances.

Tryptamine: Isomerization Involving Seven Minima. The initial studies employing SEP excitation probed conformational isomerization in tryptamine (TRA, 3-(2-aminoethyl)indole),[21,74] a molecule that differs from IPA by substitution of an NH_2 group for the COOH group of IPA. Despite the close similarity with IPA, jet-cooled TRA spreads its population over seven conformational isomers rather than two.[86−90] This circumstance presents an extraordinary challenge to conventional studies of conformational isomerization, because there are 42 distinct X → Y isomerization processes possible. In principle, the method of population transfer spectroscopy can provide upper and lower bounds to the energy barriers connecting all 42 pairs, thereby

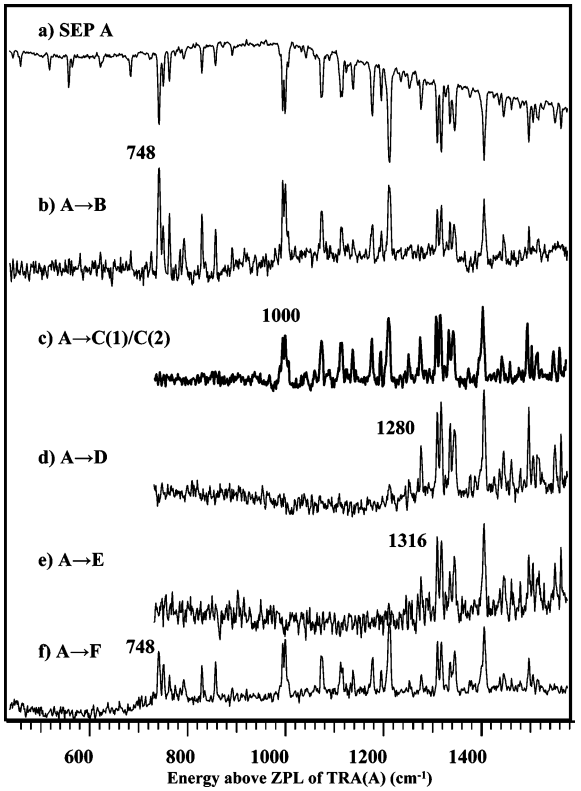

Figure 13. (a) SEP spectrum of conformer A of tryptamine (TRA). (b)−(f) Series of population transfer spectra following selective excitation of conformer A of TRA via SEP, monitoring transitions B−F due to the other product conformers. The spectrum for A → C has contributions from two conformers, which were distinguished via PT spectra recorded when monitoring distinguishing vibronic transitions in the probe step (refs 31 and 79).

constituting a complete characterization of the rate-limiting stationary points on the potential energy surface.

There are four flexible coordinates to consider in TRA: hindered rotation about the C(α)−N, C(α)−C(β), and C(β)−C(γ) bonds of the ethylamine side chain and inversion of the NH_2 group. All the low-energy isomers adopt a perpendicular configuration for the C(α)−C(β) bond relative to the indole plane, and a pyramidal configuration for the inversion coordinate. This leaves two primary flexible coordinates, C(α)−N and C(α)−C(β), both of which have 3-fold barriers. Of the resulting nine minima, two are destabilized because the nitrogen lone pair points toward the indole π cloud, leaving the seven low-lying conformational minima observed. This prototypical system has been studied in some detail by several methods, leading to a firm assignment for the seven observed $S_1 \leftarrow S_0$ origins.[86−90] The origin transitions can serve as pump wavelengths for SEP excitation of individual conformations. The most intense of these transitions is due to conformer A, labeled Gpy(out) to denote the position of the amino group (gauche on the pyrrole side of indole) and its orientation relative to the ring (lone pair pointing out away from the ring).

In Figure 13, the SEP spectrum of TRA(A) (Figure 13a) is compared with the population transfer spectra for A → B−F (Figure 13b−f).[21,74] In every case, the population transfer spectra show sharp thresholds characteristic of that reactant-product pair.

A complete characterization of all 42 pairs was hindered by the difficulty in observing the small fractional population changes in conformer Y induced by X → Y isomerization when X has a small population relative to Y. Nevertheless, the set of ten X → Y scans contributing to Figure 14 constitutes a

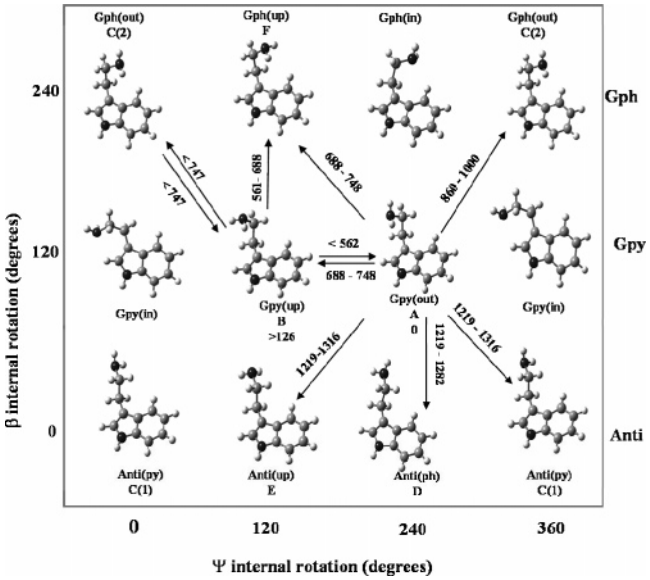

Figure 14. Experimentally determined bounds on the thresholds to isomerization for 10 reactant−product pairs of TRA, superimposed on a two-dimensional potential energy surface involving the two flexible coordinates that change the position and orientation of the NH_2 group relative to the indole ring.

substantial step forward in characterizing the potential energy surface for isomerization in TRA.

In a case like TRA, with its large number of conformers, the network of threshold measurements for individual X → Y pairs can provide insight to the efficient isomerization pathways on the multidimensional potential energy surface. For instance, a comparison of the thresholds for A → B ($688 < E_{thresh} < 748$ cm^{-1}), B → F ($566 < E_{thresh} < 688$ cm^{-1}), and A → F ($688 < E_{thresh} < 748$ cm^{-1}) suggests that the pathway from A to F passes through B. This kind of data can be extremely helpful in molecules with many flexible coordinates, where intuitive assessment of the isomerization pathways is no longer possible.

Data sets of this type provide experimental benchmarks for testing the level of theory required for ab initio calculations of conformational potentials, and the accuracies and refinements required of force fields used in simulations. Such a comparison[21] of experimental thresholds and calculated transition state energies in TRA showed a good correspondence for most X → Y pairs, with systematic differences reflecting known deficiencies of particular methods (e.g., DFT vs RIMP2). However, the experimental A → F and B → F thresholds are almost a factor of 2 lower than the calculated transition state energies for any pathways into well F.

One mechanism that would lower the experimental isomerization energy threshold below the classical barrier height is tunneling. One of the flexible coordinates in TRA involves internal rotation of the NH_2 group and therefore could be susceptible to tunneling involving the NH_2 hydrogens. To test this possibility, we measured the energy thresholds for A → B, B → F, and A → F for TRA deuterated at the NH_2 and indole NH positions. Interestingly, the measured threshold for A → B TRA(d_3), which involves NH_2 internal rotation, showed no change with deuteration, whereas the threshold for TRA(d_3) A → F was 90 cm^{-1} higher than that in TRA(h_3).[21,74] This latter result is puzzling because A → F isomerization involves motion of the entire NH_2 group between the two gauche positions, on the pyrrole and phenyl sides of indole (Figure 14). It is possible that the tunneling pathway involves inversion of the NH_2 group as it traverses the π cloud between Gpy and Gph sites. However, a final resolution to the issue still awaits theoretical work that explicitly takes tunneling into account.

Effect of Solvent on Isomerization Dynamics

The complexation of even a single water molecule to a solute has important consequences for the spectroscopy, dynamics, and reactivity of the solute. The full array of powerful tools available for exploration of the properties of isolated flexible biomolecules are equally well suited to studies of solute−$(solvent)_n$ clusters.[56,91] Supersonic expansion of a dilute mixture of solute and solvent in a buffer gas (typically helium or neon) produces solute−$(solvent)_n$ clusters cooled to within a few degrees Kelvin of absolute zero, where they can be interrogated via laser spectroscopy. When an appropriate ultraviolet chromophore is incorporated into the cluster (thereby tagging it as the "solute"), LIF and R2PI spectroscopy can be used to study the perturbations imposed on the ultraviolet chromophore by the solvent. The mass analysis afforded by R2PI spectroscopy provides a means of sorting the ultraviolet spectroscopy by cluster size. Furthermore, UV hole-burning, stimulated Raman, and IR−UV double resonance methods can provide UV,[56,91] IR,[56,91] and Raman[92] spectra of the clusters, with both size and conformation selectivity.

Because water is nature's solvent, solute−$(H_2O)_n$ clusters have received particular attention from both theory and experiment.[55,91,93−99] The combination of cooling and two-body displacement collisions typically leads to preferential formation of the most stable cluster structures downstream in the expansion. Since water is both a good H-bond donor and acceptor, the first water molecule often can bind to the solute in more than one way, especially when the solute molecule has multiple H-bonding sites.[100−103] Furthermore, the ability of water molecules to form multiple H-bonds often produces solute−$(H_2O)_n$ clusters composed of H-bonded networks, sometimes in the form of water bridges between solute donor and acceptor sites,[102,104] other times as larger $(H_2O)_n$ networks, including cycles, various 3D networks, cubes, and expanded cubes.[98,99]

When the solute molecule has conformational flexibility, the complexation of even a single water molecule can influence the solute's conformational preferences, sometimes dramatically.[55,103,105−108] In essence, the entire potential energy landscape of the "solute" is modified by the presence of the water molecule, with certain minima preferentially stabilized and others destabilized, and with new minima being formed as the solute adjusts to accommodate better H-bonds with water or between H-bonding solute sites bridged by water. Furthermore, the potential energy surface for the flexible solute−water complex incorporates all the new minima associated with water binding at various sites on the solute.

Whenever more than one conformational minimum of a given sized solute−$(solvent)_n$ cluster possesses significant population, hole-filling methods can potentially be used to study conformational isomerization between these minima. To date, these methods have been used to study two prototypical isomerization processes involving a solute−H_2O complex.[75,76] In the 3-indolepropionic acid−H_2O complex (hereafter IPA−H_2O), SEP−PT spectroscopy was used to study the effect of complexation of a water molecule on the energy barriers to isomerization of the flexible IPA molecule.[75] This study is similar in spirit to the recent elegant study of IR-induced isomerization and dissociation in the *cis/trans* naphthol-NH_3 complex by Ebata et al.[20] In the *trans*-formanilide−H_2O complex (hereafter TFA−H_2O), the isomerization event involved shuttling the complexed water molecule from one H-bonding site to another on the TFA solute.[76]

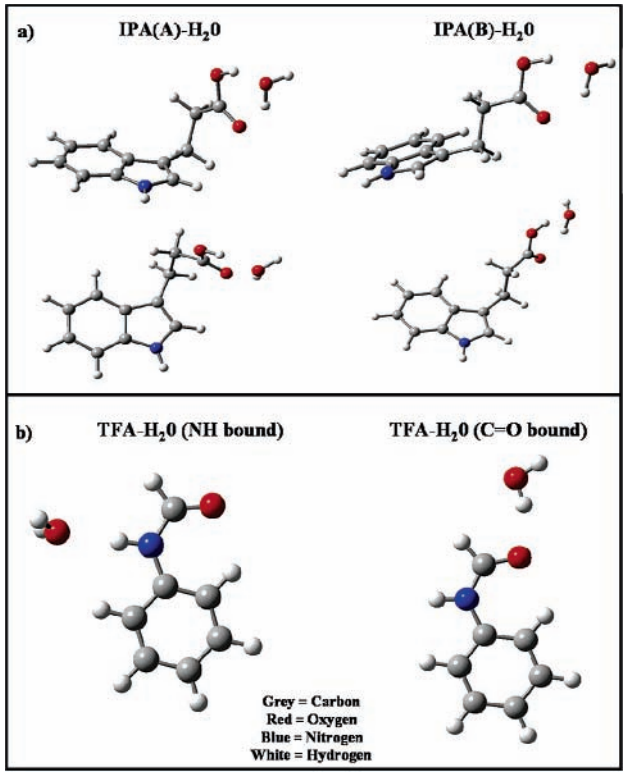

Figure 15. (a) Two observed isomers of the IPA−H_2O complex. The water molecule binds in the COOH pocket, forming a bridge between the C═O and OH groups. IPA retains the same conformations in the complex as in the monomer, providing an opportunity to study the effect of the complexed water molecule on the barrier to isomerization in IPA. (b) Two observed isomers of the *trans*-formanilide−H_2O complex.

Solute Isomerization in the Presence of Solvent: IPA−H_2O. The rotational coherence studies of Connell and Felker established that water binds preferentially to IPA by H-bonding to its COOH group, forming a doubly H-bonded bridge between the C═O and OH groups, as shown in Figure 15a).[109] The IPA−H_2O complex exists in the same two IPA conformations as the monomer, suggesting that this single water molecule has little influence on the inherent conformational energetics of the IPA *minima*.[106,109] SEP−PT spectroscopy enables the study of the influence of the bound water molecule on the *barrier* to isomerization in IPA. To probe this barrier, the IPA−H_2O complexes must be formed early in the supersonic free jet before SEP excitation occurs. If this were not the case, then it would become increasingly difficult to observe the effect of SEP excitation of the complex upstream, because many of the complexes observed downstream would be born after such excitation had already occurred. LIF excitation scans taken at the position of SEP excitation confirm that complex formation is complete there.[75] Population transfer spectra were recorded for both the IPA(A)−H_2O → IPA(B)−H_2O isomerization and its reverse, with sharp thresholds for the two processes occurring at nearly the same energies as in the IPA monomer.

As a result, the energy barriers so determined are very similar to those in the monomer (Table 1). Because the IPA(A) → IPA-(B) isomerization involves motion of the COOH group between the gauche and anti positions, the water molecule moves with the COOH group during the isomerization, only interacting with the indole ring indirectly. As a result, neither the isomerization reaction pathways nor the energy barriers to isomerization are changed significantly by the presence of the water molecule. We surmise on this basis that the intramolecular barrier in IPA is not sensitively dependent on the electronic redistribution that accompanies attachment of water to the COOH group.

Though the mode of binding of water to IPA produces little effect on the barrier to A → B isomerization in IPA, it also points the way to circumstances where the effect of water on the barriers to isomerization could be much more dramatic. For instance, if the water molecule were to form a H-bonded bridge between two flexible sites on the solute, then isomerization that changes the distance between these flexible sites would require the breaking of a H-bond with water, substantially raising the energy barrier to do so. Alternatively, depending on its point of attachment, the water molecule could raise the energies of certain minima on the surface (e.g., by steric constraints imposed by the presence of the water molecule), and hence effectively remove their participation in isomerization pathways available to the solute.

Although neither the energy threshold nor isomerization reaction path appear to have changed significantly upon addition of a single water molecule to IPA, RRKM calculations predict a slowing of the reaction rate at threshold by about a factor of 5 (Table 1). This arises because of a 5-fold increase in the vibrational density of states of the complex at threshold due to the presence of six additional low-frequency intermolecular modes in the complex. Despite this, no kinetic shift or intensity loss is observed in the SEP−PT transitions near threshold. This suggests that energy redistribution into the intermolecular modes may not be complete on the time scale of the intramolecular isomerization. Future studies will need to explore this competition between intramolecular isomerization and intermolecular energy flow more carefully, because it is of direct relevance to vibrational relaxation and isomerization in solution.

Laser-Induced Shuttling of Solvent between H-Bonding Sites on a Solute: TFA−H_2O. *trans*-Formanilide (TFA) is a phenyl derivative that incorporates a *trans*-amide group as a substituent. The carbonyl and NH sites of the *trans*-amide group point in opposite directions, and a water molecule can attach either as a H-bond donor to the carbonyl site or as a H-bond acceptor to the NH group (Figure 15b). These two isomers of the complex are formed with roughly equal populations, and have $S_1 \leftarrow S_0$ origin transitions that are well separated from one another.[100−102,110] As a result, using SEP−PTS, one can selectively excite and give well-defined amounts of internal energy to either isomer, searching for the energy thresholds for isomerizing between these sites.[76] This isomerization reaction requires the water molecule to break one H-bond with the solute and then, after translation, to form a second H-bond. The barrier probed is due to a transition state configuration in which this water molecule lies somewhere between the two sites, still interacting with the solute in a configuration far from either minimum.

We have recorded isomer-specific SEP spectra (Figure 16a) and SEP−PT spectra for the isomerization reaction starting from either isomeric reactant (NH → C═O and C═O → N−H).[76] The results starting from NH-bound TFA−H_2O are shown in Figure 16b.

Clear population gains in the product well are observed, with sharp energy thresholds for their onset. Thus, isomerization is successfully competing with vibrational cooling, even in these unusual circumstances in which the water molecule must move over regions of the TFA molecule where the traditional OH···O═C and N−H···OH_2 H-bonds are broken as water traverses the distance between the two H-bonding sites. The first observed transition in either direction occurs just below

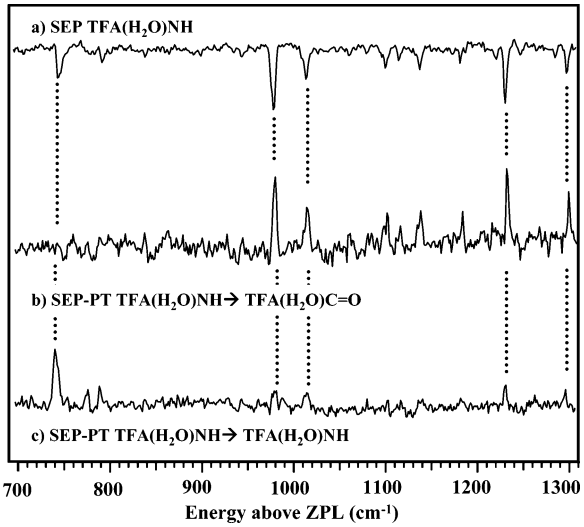

Figure 16. (a) SEP spectrum of the NH-bound TFA−H_2O complex. (b) SEP−PT spectrum for the NH → C═O isomerization channel. (c) SEP−PT spectrum for the NH → NH nonreactive channel.

1000 cm^{-1}, which is almost exactly half the binding energy of the complexes.[110] The bounds on the lowest energy barrier to isomerization in either direction, based on the first observed and last unobserved transitions, are given in Table 1. The relative energies of the two isomer minima are nearly equal, consistent with the photoion fragmentation results of Mons et al.[110]

A complementary view of the isomerization threshold (Figure 16c) is afforded by monitoring the reactant NH downstream in the expansion; that is, TFA−H_2O(NH) → TFA−H_2O(NH). In that case, the SEP dump step creates a gain in signal when transitions terminate in reactant levels that are below the isomerization threshold. However, when the isomerization threshold is exceeded, the magnitude of the gain is reduced significantly because a fraction of the excited population now isomerizes to TFA−H_2O(C═O) rather than falling back into the NH-bound TFA−H_2O reactant well.

This novel isomerization reaction raises several interesting dynamical issues. First, *ab initio* calculations have been used to identify the isomerization pathway and lowest energy transition state for the reaction. As Figure 17a shows, this pathway involves an in-plane traversal of the water molecule, passing through a transition state in which the water molecule acts as H-bond acceptor to the aldehyde C−H group. The computed energy for this transition state (1110 cm^{-1} relative to the NH-bound isomer)[76] is similar to the experimentally determined threshold (988 cm^{-1}). Second, as the energy is increased above this threshold, the water molecule can explore larger and larger regions of the surface of TFA. For instance, a second pathway in which the water molecule traverses over the top of the phenyl ring is only 200 cm^{-1} higher in energy than the in-plane pathway (Figure 17b). Thus, unlike most chemical reactions, in which reaction proceeds at higher energy by a higher flux through the same transition state, in solvent isomerization reactions, once the lowest energy threshold is exceeded, a further energy increase will quickly enable the solvent molecule to explore large regions of the intermolecular potential energy surface. Third, even at threshold, we lack a well-defined chemical intuition about the time scales for reaction. When a harmonic density of vibrational states is assumed in an RRKM calculation, a threshold time scale of 3 ns is predicted for shuttling the water molecule between the two sites (in either direction). This assumes a free exchange of energy between all vibrational modes of the complex, an assumption that needs critical evaluation. A recent theoretical study by Leitner and co-workers[111] predicts an ergodicity threshold near 1500 cm^{-1}, well above the isomerization threshold energy (~1000 cm^{-1}). This indicates that intramolecular energy flow is still restricted at threshold, and that collisions may play a crucial role in enhancing state mixing that leads to reaction.

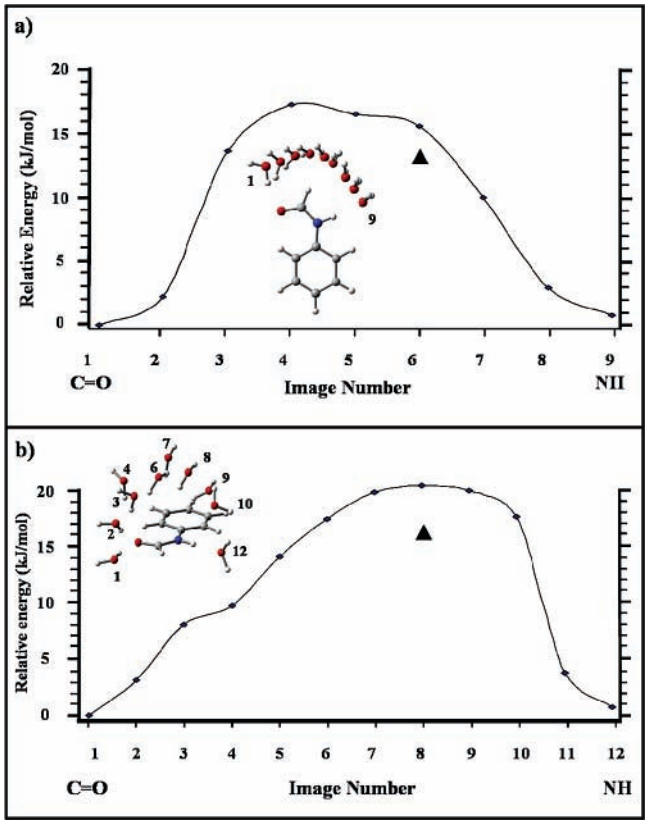

Figure 17. Nudged elastic band calculations of two minimum-energy pathways for the isomerization of a single water molecule between the NH and C═O-bound sites. (a) In-plane pathway that is the lowest-energy pathway found by calculation. (b) Second pathway about 200 cm^{-1} higher in energy involving water traversing over the top of the phenyl ring. The triangles indicate the fully converged transition state energies for the two pathways. The NEB calculations would asymptotically approach these values as tighter convergence criteria were imposed on the NEB pathway.

A Look Ahead

In this Feature Article, the experimental methods of IR- and SEP-induced population transfer spectroscopy have been introduced and applied to a series of prototypical isomerization reactions. The experimental protocol used in these studies involves initiating isomerization by selective laser excitation of a single conformation early in the expansion, followed by re-cooling the excited molecules in competition with reaction to collect the population into the various product zero-point levels for subsequent conformation-specific detection using LIF spectroscopy. The method gives up full state-to-state selection under collision-free conditions, to study larger flexible molecules and molecular clusters with complicated multidimensional potential energy surfaces with several energetically accessible minima and a large number of pathways connecting them. The hole-filling protocol can be used to determine the product yields and energy thresholds for isomerization between individual X(E) → Y reactant−product isomer pairs, each one effectively a valley-to-valley search for the most efficient isomerization

pathway. Furthermore, under certain circumstances, initial excitation is localized or partially localized in the molecule or cluster (e.g., in an XH(v=1) level), requiring energy flow into torsional or intermolecular modes before the isomerization reaction can occur. These studies thus provide a venue in which to explore whether mode-specific effects can be observed in the product quantum yields or reaction rates. A significant limitation of the method is that collisions are used as an integral part of the protocol to achieve conformation-specific detection. As a result, separating intramolecular effects from those due to collision is difficult.

There are many avenues for further research that would build effectively on the results to date.

(1) Benchmark studies of a series of molecules of direct and important biological relevance are needed. Hole-filling methods can be used to characterize the potential energy surfaces (barrier heights, relative energies of minima) in some detail, thereby providing direct experimental tests of *ab initio* methods and semiempirical force fields.

(2) These methods should be applied to tailor-made molecules that are designed to probe isomerization dynamics on specific types of potential energy surfaces (e.g., funnel, highly corrugated, etc.)[27,112] or to series of molecules that systematically vary the degree of complexity of the surface. For example, the flexibility could be spatially separated into two flexible side chains extending from either end of an aromatic ring. The potential energy landscape for such a molecule will have distinct regions due to each flexible side chain, and unique regions associated with the interaction of the two chains. The dynamics of isomerization in double-chain molecules such as this has a potential to show conformation-specific and mode-specific effects. One could imagine that initiating conformational isomerization via a vibration localized in one chain might favor isomerization events within that chain, even if lower energy pathways are present in the opposite chain. Alternatively, localized excitation could be accomplished via SEP by studying bichromophore molecules in which two nearly-identical, but weakly coupled, UV chromophores are placed at either end of a single flexible chain. Then, SEP can be used to initiate isomerization via Franck−Condon factors involving levels localized in one or the other aromatic ring, so that energy flow that leads to conformational isomerization occurs selectively in one or the other direction along the chain.

(3) There is the exciting prospect of applying these methods or adaptations of them to isomerization when the flexible sites are near to radical sites or charges, where much less is known about the barrier heights than in stable neutral molecules. The recent elegant high-resolution LIF studies of alkoxy radicals by Miller and co-workers provide a spectroscopic foundation for such work.[113−117]

(4) The demonstrated ability of the method to explore solvent motion about a solute (e.g., H_2O shuttling between the two H-bonding sites of *trans*-formanilide)[76] suggests its application to complexes and clusters where a wider range of solvent motions is possible. For instance, in cases where two solvent molecules form a bridge between H-bonding sites on an aromatic solute, they could undergo a solvent-swapping reaction in which the barrier for exchange of positions of the solvents could be studied. Alternatively, if both solute and solvent have flexible sites, isomerization within the flexible solute will occur in competition with isomerization in the solvent. This latter process requires energy flow through the intermolecular bonds into the intramolecular modes of the solvent, which, if impeded, could lead to product distributions not dictated by barrier heights alone.

(5) The competition between intramolecular and intermolecular processes also could effect the dissociation of the complex. For example, in a flexible biomolecule−H_2O complex such as tryptamine−H_2O,[107,108] when laser excitation exceeds the dissociation threshold, the flexible product molecule can end up in one of several conformational product wells.[86−90] If dissociation occurs fast compared to isomerization, the initial "landing point" on the bare molecule potential energy surface will be dictated by the geometry of the complex. Alternatively, if isomerization within the solute molecule precedes dissociation, it would lead to a range of conformational products dictated by the potential energy surface for the isomerization.[21]

(6) Finally, methods need to be developed for extracting absolute, energy-dependent isomerization rates for specific X → Y reactant-product pairs. The observed product yields result from a competition between isomerization and collisional cooling (see eqs 7 and 8), varying from thermodynamic to kinetic control as the cooling rate increases. The collision rate and energy lost per collision can be changed by varying the point of SEP excitation in the expansion, the backing pressure, and the nature of the bath gas, whereas the energy above the threshold is chosen by the dump laser wavelength.

In all these circumstances, a close connection with theory will be crucial to extracting the maximum physical insight to the dynamics of isomerization in flexible molecules and molecular clusters. It is hoped that such studies will forge a useful pathway into the complexity gap that separates small molecules from the large macromolecules and solvent surroundings that accompany the functioning of bioactive molecules in aqueous solution.

Acknowledgment. I gratefully acknowledge financial support for this research from the National Science Foundation (CHE-0242818). The work on *meta*-ethynylstyrene was supported by the Department of Energy Basic Energy Sciences (DE-FG02-96ER14656). This research would not have been possible without the hard work of several members of the Zwier group, including Jasper Clarkson, Dr. Brian Dian, Dr. Gina Florio, Dr. Asier Longarte, and Talitha Selby. We have also benefited greatly from collaborations with the theory groups of Ken Jordan, David Wales, and David Leitner.

References and Notes

(1) Polanyi, J. C. *Angew. Chem., Int. Ed.* **1987**, *26*, 952−971.
(2) Herschbach, D. R. *Angew. Chem., Int. Ed.* **1987**, *26*, 1221−1243.
(3) Lee, Y. T. *Angew. Chem., Int. Ed.* **1987**, *26*, 939−951.
(4) Orr-Ewing, A. J.; Zare, R. N. *Annu. Rev. Phys. Chem.* **1994**, *45*, 315−366.
(5) Polanyi, J. C. *Science* **1987**, *236*, 680−690.
(6) Lee, Y. P. *Annu. Rev. Phys. Chem.* **2003**, *54*, 215−244.
(7) Butkovskaya, N. I.; Setser, D. W. *Int. Rev. Phys. Chem.* **2003**, *22*, 1−72.
(8) Fernandez-Alonso, F.; Zare, R. N. *Annu. Rev. Phys. Chem.* **2002**, *53*, 67−99.
(9) Brouard, M.; O'Keeffe, P.; Vallance, C. *J. Phys. Chem. A* **2002**, *106*, 3629−3641.
(10) Callegari, A.; Rizzo, T. R. *Chem. Soc. Rev.* **2001**, *30*, 214−225.
(11) Valentini, J. J. *Annu. Rev. Phys. Chem.* **2001**, *52*, 15−39.
(12) Herschbach, D. *Annu. Rev. Phys. Chem.* **2000**, *51*, 1−39.
(13) Simons, J. P. *Faraday Discuss.* **1999**, *113*, 1−25.
(14) Crim, F. F. *Acc. Chem. Res.* **1999**, *32*, 877−884.
(15) Weisshaar, J. C.; Zwier, T. S.; Leone, S. R. *J. Chem. Phys.* **1981**, *75*, 4873−4884.
(16) Green, D.; Hammond, S.; Keske, J.; Pate, B. H. *J. Chem. Phys.* **1999**, *110*, 1979.
(17) McWhorter, D. A.; Hudspeth, E.; Pate, B. H. *J. Chem. Phys.* **1999**, *110*, 2000−2009.
(18) Gruebele, M.; Wolynes, P. G. *Acc. Chem. Res.* **2004**, *37*, 261−267.

(19) Leitner, D. M.; Levine, B.; Quenneville, J.; Martinez, T. J.; Wolynes, P. G. *J. Phys. Chem. A* **2003**, *107*, 10706−10716.
(20) Ebata, T.; Kouyama, K.; Mikami, N. *J. Chem. Phys.* **2003**, *119*, 2947−2950.
(21) Clarkson, J. R.; Dian, B. C.; Moriggi, L.; DeFusco, A.; McCarthy, V.; Jordan, K. D.; Zwier, T. S. *J. Chem. Phys.* **2005**, *122*, 214311.
(22) Csontos, J.; Kalman, M.; Tasi, G. *J. Mol. Struct.−THEOCHEM* **2003**, *640*, 69−77.
(23) Cornell, W. D.; Cieplak, P.; Bayly, C. I.; Gould, I. R.; Merz, K. M., Jr.; Ferguson, D. M.; Spellmeyer, D. C.; Fox, T.; Caldwell, J. W.; Kollman, P. A. *J. Am. Chem. Soc.* **1995**, *117*, 5179−5197.
(24) Kollman, P.; Dixon, R.; Cornell, W.; Fox, T.; Chipot, C.; Pohorille, A. *Comput. Sim. Biomol. Syst.* **1997**, *3*, 83.
(25) Evans, D.; Wales, D.; Dian, B. C.; Zwier, T. S. *J. Chem. Phys.* **2004**, *120*, 148−157.
(26) Becker, O. M.; Karplus, M. *J. Chem. Phys.* **1997**, *106*, 1495−1517.
(27) Wales, D. J.; Doye, J. P. K.; Miller, M. A.; Mortenson, P. N.; Walsh, T. R. Energy Landscapes: From Clusters to Biomolecules. In *Advances in Chemical Physics*; Prigogine, I., Rice, S. A., Eds.; Wiley & Sons: New York, 2000; Vol. 115, pp 1−111.
(28) Mortenson, P. N.; Wales, D. J. *J. Chem. Phys.* **2001**, *114*, 6443−6454.
(29) Karplus, M. *Folding Design* **1997**, *2*, S69−S75.
(30) Gruebele, M. *Curr. Opin. Struct. Biol.* **2002**, *12*, 161−168.
(31) Baer, T.; Potts, A. R. *J. Phys. Chem. A* **2000**, *104*, 9397−9402.
(32) Leitner, D. M. *Int. J. Quantum Chem.* **1999**, *75*, 523−531.
(33) Bigwood, R.; Gruebele, M.; Leitner, D. M.; Wolynes, P. G. *Proc. Natl. Acad. Sci. U.S.A.* **1998**, *95*, 5960−5964.
(34) Bigwood, R. M.; Gruebele, M. *J. Mol. Struct.−THEOCHEM* **2002**, *589*, 447−457.
(35) Gruebele, M.; Bigwood, R. *Int. Rev. Phys. Chem.* **1998**, *17*, 91−145.
(36) Yu, X.; Leitner, D. M. *J. Phys. Chem. B* **2003**, *107*, 1698−1707.
(37) Kay, L. E. *J. Magn. Reson.* **2005**, *173*, 193−207.
(38) Kern, D.; Eisenmesser, E. Z.; Wolf-Watz, M. Enzyme dynamics during catalysis measured by NMR spectroscopy. In *Nuclear Magnetic Resonance of Biological Macromolecules, Part C*; Elsevier: Amsterdam, 2005;Vol. 394, pp 507−524.
(39) Jacob, J.; Krantz, B.; Dothager, R. S.; Thiyagarajan, P.; Sosnick, T. R. *J. Mol. Biol.* **2004**, *338*, 369−382.
(40) Fraser, G. T.; Suenram, R. D.; Lugez, C. L. *J. Phys. Chem. A* **2000**, *104*, 1141−1146.
(41) Mate, B.; Suenram, R. D.; Lugez, C. *J. Chem. Phys.* **2000**, *113*, 192−199.
(42) Mikhonin, A. V.; Myshakina, N. S.; Bykov, S. V.; Asher, S. A. *J. Am. Chem. Soc.* **2005**, *127*, 7712−7720.
(43) Jeffrey, G. A.; Saenger, W. *Hydrogen Bonding in Biological Structures*; Springer-Verlag: New York, 1991.
(44) Latajka, Z.; Scheiner, S. *Chem. Phys. Lett.* **1990**, *174*, 179−184.
(45) Krummel, A. T.; Mukherjee, P.; Zanni, M. T. *J. Phys. Chem. B* **2003**, *107*, 9165−9169.
(46) Gerlach, A.; Unterberg, C.; Fricke, H.; Gerhards, M. *Mol. Phys.* **2005**, *103*, 1521−1529.
(47) Chung, H. S.; Khalil, M.; Smith, A. W.; Ganim, Z.; Tokmakoff, A. *Proc. Natl. Acad. Sci. U.S.A.* **2005**, *102*, 612−617.
(48) Londergan, C. H.; Kim, Y. S.; Hochstrasser, R. M. *Mol. Phys.* **2005**, *103*, 1547−1553.
(49) Kim, Y. S.; Wang, J. P.; Hochstrasser, R. M. *J. Phys. Chem. B* **2005**, *109*, 7511−7521.
(50) Kim, Y. S.; Hochstrasser, R. M. *J. Phys. Chem. B* **2005**, *109*, 6884−6891.
(51) Wright, J. C. *Vibr. Spectrosc.* **2004**, *36*, 179−184.
(52) Callis, P. R.; Burgess, B. K. *J. Phys. Chem. B* **1997**, *101*, 9429−9432.
(53) Chen, Y.; Barkley, M. D. *Biochemistry* **1998**, *37*, 9976−9982.
(54) Crespo-Hernandez, C. E.; Cohen, B.; Hare, P. M.; Kohler, B. *Chem. Rev.* **2004**, *104*, 1977−2019.
(55) Robertson, E. G.; Simons, J. P. *Phys. Chem. Chem. Phys.* **2001**, *3*, 1−18.
(56) Zwier, T. S. *J. Phys. Chem. A* **2001**, *105*, 8827−8839.
(57) Dian, B. C.; Longarte, A.; Mercier, S.; Evans, D.; Wales, D. J.; Zwier, T. S. *J. Chem. Phys.* **2002**, *117*, 10688−10702.
(58) Plutzer, C.; Kleinermanns, K. *Phys. Chem. Chem. Phys.* **2002**, *4*, 4877−4882.
(59) Nir, E.; Janzen, C.; Imhof, P.; Kleinermanns, K.; deVries, M. S. *J. Chem. Phys.* **2001**, *115*, 4604−4611.
(60) Fricke, H.; Gerlach, A.; Unterberg, C.; Rzepecki, P.; Schrader, T.; Gerhards, M. *Phys. Chem. Chem. Phys.* **2004**, *6*, 4636−4641.
(61) Chin, W.; Compagnon, I.; Dognon, J. P.; Canuel, C.; Piuzzi, F.; Dimicoli, I.; von Helden, G.; Meijer, G.; Mons, M. *J. Am. Chem. Soc.* **2005**, *127*, 1388−1389.
(62) Chin, W.; Dognon, J. P.; Canuel, C.; Piuzzi, F.; Dimicoli, I.; Mons, M.; Compagnon, I.; von Helden, G.; Meijer, G. *J. Chem. Phys.* **2005**, *122*, 2696−2706.
(63) Dian, B. C.; Longarte, A.; Zwier, T. S. *J. Chem. Phys.* **2003**, *118*, 2696−2706.
(64) Chin, W.; Mons, M.; Dognon, J. P.; Mirasol, R.; Chass, G.; Dimicoli, I.; Piuzzi, F.; Butz, P.; Tardivel, B.; Compagnon, I.; von Helden, G.; Meijer, G. *J. Phys. Chem. A* **2005**, *109*, 5281−5288.
(65) Gerhards, M. *Opt. Commun.* **2004**, *241*, 493−497.
(66) Choi, M. Y.; Dong, F.; Miller, R. E. *Philos. Trans. R. Soc. London A* **2005**, *363*, 393−412.
(67) Nir, E.; Imhof, P.; Kleinermanns, K.; Vries, M. S. d. *J. Am. Chem. Soc.* **2000**, *122*, 8091−8092.
(68) Abo-Riziq, A. G.; Crews, B.; Bushnell, J. E.; Callahan, M. P.; De Vries, M. S. *Mol. Phys.* **2005**, *103*, 1491−1495.
(69) Chin, W.; Mons, M.; Dognon, J. P.; Piuzzi, F.; Tardivel, B.; Dimicoli, I. *Phys. Chem. Chem. Phys.* **2004**, *6*, 2700−2709.
(70) Chin, W.; Dognon, J. P.; Piuzzi, F.; Tardivel, B.; Dimicoli, I.; Mons, M. *J. Am. Chem. Soc.* **2005**, *127*, 707−712.
(71) Dian, B. C.; Longarte, A.; Zwier, T. S. *Science* **2002**, *296*, 2369−2373.
(72) Dian, B. C.; Longarte, A.; Winter, P. R.; Zwier, T. S. *J. Chem. Phys.* **2004**, *120*, 133−147.
(73) Dian, B. C.; Florio, G. M.; Clarkson, J. R.; Longarte, A.; Zwier, T. S. *J. Chem. Phys.* **2004**, *120*, 9033−9046.
(74) Dian, B. C.; Clarkson, J. R.; Zwier, T. S. *Science* **2004**, *303*, 1169−1173.
(75) Clarkson, J. R.; Baquero, E.; Zwier, T. S. *J. Chem. Phys.* **2005**, *122*, 214312.
(76) Clarkson, J. R.; Baquero, E.; Shubert, V. A.; Myshakin, E. M.; Jordan, K. D.; Zwier, T. S. *Science* **2005**, *307*, 1443−1446.
(77) Selby, T. M.; Clarkson, J. R.; Mitchell, D.; Fitzpatrick, J. A. J.; Lee, H. D.; Pratt, D. W.; Zwier, T. S. *J. Phys. Chem. A* **2005**, *109*, 4484−4496.
(78) Florio, G. M.; Christie, R.; Jordan, K. D.; Zwier, T. S. *J. Am. Chem. Soc.* **2002**, *124*, 10236−10247.
(79) Barker, J. R. *J. Phys. Chem.* **1984**, *88*, 11−18.
(80) Troe, J. *Pure Appl. Chem.* **1997**, *69*, 841−846.
(81) Damm, M.; Deckert, F.; Hippler, H.; Troe, J. *J. Phys. Chem.* **1991**, *95*, 2005−2009.
(82) Flynn, G. W.; Parmenter, C. S.; Wodtke, A. M. *J. Phys. Chem.* **1996**, *100*, 12817−12838.
(83) Leitner, D. M.; Wolynes, P. G. *J. Chem. Phys.* **1996**, *105*, 11226−11236.
(84) Leitner, D. M.; Wolynes, P. G. *J. Phys. Chem. A* **1997**, *101*, 541−548.
(85) Schroeder, J.; Steinel, T.; Troe, J. *J. Phys. Chem. A* **2002**, *106*, 5510−5516.
(86) Nguyen, T. V.; Korter, T. M.; Pratt, D. W. *J. Mol. Spectrosc.*, in press.
(87) Wu, Y. R.; Levy, D. H. *J. Chem. Phys.* **1989**, *91*, 5278−5284.
(88) Philips, L. A.; Levy, D. H. *J. Chem. Phys.* **1988**, *89*, 85−90.
(89) Carney, J. R.; Zwier, T. S. *J. Phys. Chem. A* **2000**, *104*, 8677−8688.
(90) Carney, J. R.; Zwier, T. S. *Chem. Phys. Lett.* **2001**, *341*, 77−85.
(91) Zwier, T. S. *Annu. Rev. Phys. Chem.* **1996**, *47*, 205−241.
(92) Felker, P. M. *Chem. Rev.* **1994**, *94*, 1784.
(93) Gruenloh, C. J.; Carney, J. R.; Hagemeister, F. C.; Arrington, C. A.; Zwier, T. S.; Fredericks, S. Y.; Wood, J. T.; Jordan, K. D. *J. Chem. Phys.* **1998**, *109*, 6601−6614.
(94) Janzen, C.; Spangenberg, D.; Roth, W.; Kleinermanns, K. *J. Chem. Phys.* **1999**, *110*, 9898−9907.
(95) Kim, K. S.; Tarakeshwar, P.; Lee, J. Y. *Chem. Rev.* **2000**, *100*, 4145−4185.
(96) Clary, D. C.; Benoit, D. M.; Van Mourik, T. *Acc. Chem. Res.* **2000**, *33*, 441−447.
(97) Muller-Dethlefs, K.; Hobza, P. *Chem. Rev.* **2000**, *100*, 143−167.
(98) Roth, W.; Schmitt, M.; Jacoby, C.; Spangenberg, D.; Janzen, C.; Kleinermanns, K. *Chem. Phys.* **1998**, *239*, 1−9.
(99) Zwier, T. S. The Infrared spectroscopy of hydrogen-bonded clusters: Cycles, chains, cubes, and three-dimensional networks. In *Advances in Molecular Vibrations and Collision Dynamics*; Bowman, J. M., Bacic, Z., Eds.; JAI Press: Greenwich, 1998; Vol. 3, pp 249−280.
(100) Fedorov, A. V.; Cable, J. R. *J. Phys. Chem. A* **2000**, *104*, 4943−4952.
(101) Robertson, E. G. *Chem. Phys. Lett.* **2000**, *325*, 299−307.
(102) Dickinson, J. A.; Hockridge, M. R.; Robertson, E. G.; Simons, J. P. *J. Phys. Chem. A* **1999**, *103*, 6938−6949.
(103) Florio, G. M.; Zwier, T. S. *J. Phys. Chem. A* **2003**, *107*, 974−983.
(104) Bach, A.; Coussan, S.; Muller, A.; Leutwyler, S. *J. Chem. Phys.* **2000**, *113*, 9032−9043.

(105) Peteanu, L. A.; Levy, D. H. *J. Phys. Chem.* **1988**, *92*, 6554−6561.

(106) Carney, J. R.; Dian, B. C.; Florio, G. M.; Zwier, T. S. *J. Am. Chem. Soc.* **2001**, *123*, 5596−5597.

(107) Nguyen, T. V.; Pratt, D. W. Submitted for publication.

(108) Schmitt, M.; Bohm, M.; Ratzer, C.; Vu, C.; Kalkman, L.; Meerts, W. L. *J. Am. Chem. Soc.* **2005**, *127*, 10356−10364.

(109) Connell, L. L. Structural Studies of Hydrogen-bonded Clusters using Rotational Coherence Spectroscopy, University of California at Los Angeles, 1991.

(110) Mons, M.; Dimicoli, I.; Tardivel, B.; Piuzzi, F.; Robertson, E. G.; Simons, J. P. *J. Phys. Chem. A* **2001**, *105*, 969−973.

(111) Leitner, D. M. Personal communication.

(112) Evans, D. A.; Wales, D. J. *J. Chem. Phys.* **2003**, *118*, 3891−3897.

(113) Tarczay, G.; Zalyubovsky, S. J.; Miller, T. A. *Chem. Phys. Lett.* **2005**, *406*, 81−89.

(114) Zu, L.; Liu, J. J.; Gopalakrishnan, S.; Miller, T. A. *Can. J. Chem.—Rev. Can. Chim.* **2004**, *82*, 854−866.

(115) Zu, L.; Liu, J. J.; Tarczay, G.; Dupre, P.; Miller, T. A. *J. Chem. Phys.* **2004**, *120*, 10579−10593.

(116) Gopalakrishnan, S.; Zu, L.; Miller, T. A. *J. Phys. Chem. A* **2003**, *107*, 5189−5201.

(117) Gopalakrishnan, S.; Carter, C. C.; Zu, L.; Stakhursky, V.; Tarczay, G.; Miller, T. A. *J. Chem. Phys.* **2003**, *118*, 4954−4969.